A Spatiotemporal Communication Architecture for Fiber Optic Few-Mode Systems

A Thesis

Presented to

the faculty of the School of Engineering and Applied Science

University of Virginia

in partial fulfillment

of the requirements for the degree

Master of Science

by

Emeka V. Ikpeazu, Jr.

April

2019

Abstract

Optical fibers are ubiquitous in today's communication networks and are even becoming more prevalent thanks to their promising features such as low loss, high-bandwidth, and high security. Optical fiber has already done a lot to facilitate the fast transmission of information across long distances. Such technology is different than communication systems of old and the wireless network systems of today. For example, optical fiber affords a user more reliability and security while RF systems retain a susceptibility to jamming and eavesdropping that must be mitigated. In the last half-century, a revolution has occurred in the field of communication systems. Subsequently, the facilitation of optical transmission has emerged in the domains of time, wavelength, mode, and "code" among many others. Mode-division multiplexing (MDM) is one way to improve optical throughput through fibers creating multiple channels of communication.

This thesis addresses the detection and sorting of optically transmitted information that makes use of a spatial MDM scheme but also combines it with a standard communications model to create a spatiotemporal system. The challenge herein is to devise a scheme that combines the temporal aspect of communication systems with the spatial profile of the electric field that also carries the information. We take advantage of the fiber's cross-section which consequently allows us to model each mode profile as an "image" and sample it accordingly using a photodetector array. This architecture makes use of a quasi-orthogonal mode model with user coupling among each mode. In this way, we can create an integrative communication architecture that incorporates the coupling between users. We also propose a robust way of multiuser detection that recovers *all* user input bitstreams and optimizes the way in which users are positioned for the best system performance.

For my Mom, Dad, and my Grandfather, the late Josiah Udeaham nwa-Ohiaeri

Ọ ga-adili gị mma,
Naba na ndokwa

Acknowledgements

I am greatly indebted to my advisor Dr. Maïté Brandt-Pearce for assisting me and helping me through this work, her patience for me and her willingness to encourage my success is inimitable. She assisted me in roadblocks and helped my work progress, even as I went through my tough academic times. I am happy to have worked with her for my master's work and I hope to continue to work with her.

Professors Andreas Beling and Stephen Wilson also deserve credit for being on my committee. I appreciate being a student of Professor Beling and his work in teaching me optical communication devices in his course. It was very helpful and I would recommend it to anyone who is interested in optical communications. It was a very good course on how physics can be directed towards higher level applications. Professor Wilson has been very helpful for me as well as he was the person with whom I toured UVa. He was also the person who allowed me to be admitted into the Masters of Engineering program when I got rejected for the PhD program. I am grateful that he saw my potential and continues to see it through my performance in his classes and my participation in the ECE graduate council.

My group partners were also very instrumental in helping me complete this thesis work. I consulted them when my algorithms were slow. They helped me with improving the processing speed of my MATLAB programs. My group partners Emmanuel Denloye-Ito and Hamid Hosseinianfar and my friends Tannaz Farrahi, Jesse Morgan, and others were helpful for my work to continue when I hit a roadblock in this work. They were of good assistance whenever I needed them.

I would also like to thank the National Science Foundation for giving me the funding to do this work and paying a significant part for my graduate education. I am grateful for being under Professor Brandt-Pearce's grant and sponsorship.

Last but not least, I would also like to thank my parents who have encouraged me throughout my work here. I am so happy to have them call me and ask how I am doing. I am thankful for their help and constant support in difficult periods I have faced here.

Table of Contents

List of Acronyms

ADC: Analog-to-digital converter

AO: Adaptive optics

ASK: Amplitude-shift keying

AWGN: Additive white Gaussian noise

EMI: Electromagnetic interference

FIFO: Few-input-few-output

FMF: Few-mode fiber

FSK: Frequency-shift keying

FWHM: Full-width half-maximum

IL: Insertion loss

I/O: Input-output

ISI: Intersymbol interference

LAN: Local area network

MCF: Multicore fiber

MDM: Mode-division multiplexing

MIMO: Multiple-input-multiple-output

MMF: Multimode fiber

OOK: On-off keying

PSK: Phase-shift keying

RZ: Return-to-zero

SDM: Spatial-division multiplexing

SER: Symbol error rate

SISO: Single-input-single-output

SMF: Single-mode fiber

SNR: Signal-to-noise ratio

TDMA: Time-division multiple access

Table of Figures

List of Tables

Chapter 1: Introduction

Transmission speed is already very fast with Ethernet 5 cable reaching information transmission rates of between 10^8 and 10^9 bits/s. The record so far for a multicore fiber is $1.05 \cdot 10^{15}$ bits/s [1]. Many fiber optic development methods and schemes are for the most part directed toward what happens before the fiber or along the fiber, (e.g. precoding [2] or iterated amplifiers). In this work, we are developing a multiuser mode-division multiplexing method for the receiver at the end of a length of optical fiber, using a spatiotemporal mode-pulse profile of the signal to examine what happens at the receiver at the end of a length of optical fiber, particularly what happens with a spatiotemporal mode-pulse profile when it interacts with a photodetector sensor grid.

Optical modes are forms taken by the guided waves that are allowed to propagate in a waveguide under a certain set of conditions. These conditions have to do with the indices of refraction of the core and cladding, which is a function of the materials of which they are composed, the dimensions of the waveguide, and the wavelength being transmitted. Our model deals with circular waveguides, or fibers. These modes propagate at different angles and velocities as they reflect off the core-cladding interface throughout the fiber. We already know that single mode fibers have no capacity for mode-division multiplexing (MDM). On the other hand, however, we already know that using multimode fibers (MMFs) decreases the spectral width of the output [3]. This is especially true in the context of multiuser mode-division multiplexing (MDM) [4]. For the sake of finding a balance between these two extremes and for simplicity, our model makes use of a few-mode fiber.

In optical fiber communication and contemporary communications in general we mostly deal with temporal pulses as conduits for information transmission. In the same way that digitization has facilitated the modernization of such communication systems, one can apply this idea to spatial profiles of optical fields. Furthermore, two ongoing challenges in the field of optical fiber communications are the issues of speed and reliability. High speed communications applications exacerbate these issues indefinitely.

In this thesis we will take advantage of photodetection technologies in order to capture the spatial profile mode. These sensors take the form of photodetector grids that function as spatial samplers. This will be combined with the temporally-based architecture of modern communication systems. The mechanisms according to which our optical fiber system functions are rather simple: a light source, optical fiber, detector element, and our decision maker. Moreover, one can divide the types of fiber optic sensors into the type of modulation scheme that an optical signal undergoes. In this way, optical detector systems are classified by property used for multiplexing (e.g. intensity, temporal delay, spectrum, polarization, etc.) For this thesis, the primary medium we will be exploring are intensity sensors for non-coherent (direct) detection, of which more will be said later in this work.

1.1 Fiber Optic Modal Sampling

The model of photodetector grids that is considered in this work can be divided into two parts. The first part deals with optical fiber modal sampling, i.e., spatial sampling. The second part has to do with matched filters corresponding to mode-division multiplexing (MDM) encoding schemes. Such grids have been crafted in order to maximize coupling efficiency for the optical fiber. This is mainly done by integration with the waveguide or fiber and a quantum efficiency of 80% can be achieved [5]. But today this efficiency can be improved through signal enhancement circuitry [6]. In the 1970s these photodiodes would have a response time of around 20 microseconds. Today ultrafast photodiodes have response times on the order of picoseconds (10^{-12} s), good enough for rigorous pulse-sampling [7]. Today's optical fiber communication systems work the same way as a temporal pulse-based system because information is encoded in a series of sequential pulses and most systems use single mode fibers (SMFs). However, using the fast temporal response of photodiodes and assembling them into a grid can create a new path towards a hybrid system of space and time. That is, the integration of MDM and OOK for Gaussian pulses.

Sptatio-temporal processing in optical systems already has precedent in adaptive optics (AO) and astrophotonic systems. Such systems compensate for wavefront distortion that is likely to occur in the context of atmospheric aberration in radio-astronomy applications [8]. This aberration can be simulated in using rotating specular (rough) transmission lenses. However, the wavefront correction apparatus is too slow for our means as it works the same way as a charge-coupled device. Such devices integrate the "image" over an exposure time t_e on the order of milliseconds [8]. Such a time is not fast enough for our purposes here. What is necessary here is a spatial receiver with an integrative element that allows for high temporal resolution pulse-sampling [9,10]. The necessary sampling would be such that it finds observations in contemporary high-speed time-division multiple access (TDMA) applications and can therefore accommodate a large optical spectrum [11]. Additionally, our goal is to go from analog to digital in both space and time. In this way, what is needed is a is an element that can function as a spatial analog-to-digital converter (ADC). In this work, we use a grid of microphotodiodes as an optical sensing and sampling apparatus. In this way, the spatial profile will undergo spatial digitization.

Advances in fiber optic detection technologies in the last thirty years have caused the prices of such equipment to drop tremendously and so such devices are available for use in the near future if not contemporary use [12]. The method proposed in this thesis would have to make use of photodiodes for efficient sampling and space and time which can very well be achieved as response time τ is linearly proportional to diode capacitance, which is in turn linearly proportional to device area [13]. Now the challenge stands to use these efficient technologies for the purpose of reliable and fast data transmission.

1.2 The Role of the Optical Fiber

We first begin with coupling light into the fiber to stimulate the various modes, which is especially important in the context of having multiple users. Parallel encoding schemes are a novel and efficient way of increasing data transmission rates. Given that in this research we experiment with spatially sampled modes, we will examine the role of a "high-resolution"—oversampled—microphotodiode sensing grid.

The optical fiber allows for modes which propagate at different velocities and angles throughout the fiber [14] due to the effects of dispersion. MMFs are also easier to work with anyway, as splicing alignments and microfabrication errors are not as costly to the overall performance. The thrust of MMFs in this regard is to exploit the benefits of informational encoding as it relates to the various modes that are carried in a particular fiber. Optical traffic demands are more easily met, at least in theory, where there is the assumption of perfect or almost perfect orthogonality. However, that is never really the case. Not only is there modal coupling, but the effects of dispersion cause the pulses to accrue delays and the bit streams to overlap, leading to intersymbol interference (ISI). Illustrated in Figure 1.1 is a look at the various stages of bit overlap over the course of an optical fiber.

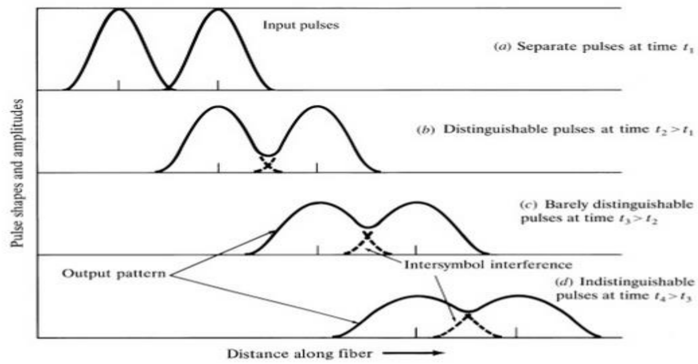

Figure 1.1: Dispersion over the length of an optical fiber pulse envelope in time, which causes ISI [15].

The overall template that we use here is that of a typical analog transceiver model. The first step is the information source, an external beam that converts information in to a series pulses to be sent down the fiber. The information is principally encoded in the “variations” of a particular property of the signal. This is known as optical modulation and it can take place in several domains; the most common, however, phase shift-keying (PSK) and amplitude shift-keying (ASK). The primary medium for modulation in this thesis will be ASK, particularly in on-off keying (OOK), a scheme for binary amplitude modulation; however, such methods can be generalized to more inclusive alphabets, i.e., *M*-ary modulation. Overall, the model we propose is an optical realization of the block diagram represented in Figure 1.2.

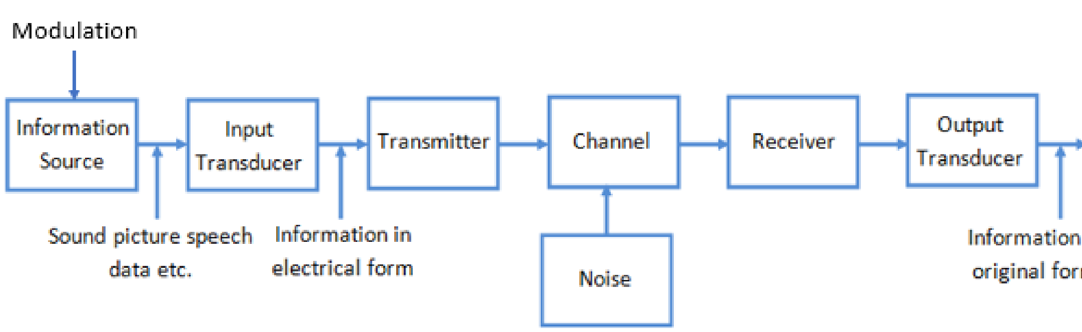

Figure 1.2: A rough diagram of the structure of a typical transceiver communication system.

External modulation encodes information onto a beam source to be sent down a fiber. The optical signal is subject to noise at the square-law detector receiver. The stimulation of modes by a broadband (Gaussian) source means that encoding modulate the allowable modes to varying degrees.

1.3 Review of Fiber Optic Mode Theory

We must first review fiber optic mode theory to understand how communication systems can effectively take advantage of optical physics. Modes are the means by which we communicate information in this system. These modes are the solutions to the Helmholtz wave equation in cylindrical coordinates subject to the conditions of the fiber and they propagate in the *z*-direction [14]. Helmholtz's equation is expressed as:

$$\nabla^2\vec{\boldsymbol{E}}(r,\phi) + k_0^2 n^2 \vec{\boldsymbol{E}}(r,\phi) = 0 \tag{1.1}$$

where k_0 is the wavenumber $2\pi/\lambda$, $\vec{\boldsymbol{E}}$ is the electric field, r is its radial component, ϕ is its azimuthal component, and n is the index of refraction

Additionally, these modes are both guided (confined in the fiber) and radiative (not confined in the fiber). For the purposes of our analysis, the effect of radiation modes, unguided modes that do not have a discrete spectrum, will be neglected. User information will only be attached to the stimulated *guided* modes of the fiber. What mainly distinguishes the various modes that propagate in the fiber is the wavenumber in the z-direction, β. However, sometimes the guided modes can have the same (or approximately the same) β-value. In such a case these modes come together to form a mode group. These mode groups become especially active in the context of the weakly-guiding approximation, where the index of the core is only *slightly* higher than that of the cladding. We can make this approximation to form linear combinations of modes in the fiber. The degree to which an mode $LP_{\nu m}$ is stimulated is shown in the equation below:

$$c_{\nu m} = \frac{\int E_i(r,\phi) \cdot E_{\nu m}(r,\phi) dA}{\int |E^*_{\nu m}(r,\phi) \cdot E_{\nu m}(r,\phi)| dA} \tag{1.2}$$

where, $E_i(r,\phi)$ is the input field—a cylindrical Laguerre-Gaussian beam in this case—and $E_{\nu m}(r,\phi)$ is the optical field profile for the LP$_{\nu m}$, ν is the azimuthal index, m is the radial index, and $LP_{\nu m}$ is the linearly polarized eigenmode for the fiber. The modulated modes are thus written as the following sum

$$E(r,\phi,z=0,t) = \sum_{m=1}^{M} \sum_{n=1}^{N} b_m c_n \, E_n(r,\phi,z=0,t-mT_b-\tau_n) \tag{1.3}$$

N is the number of different modes in the fiber, c_n is the excitation amplitude for the *n*th mode, b_m is the *m*th bit of the bitstream, T_b is the bit period, τ_n is the waveguide delay for mode *n*, and *M* is number of bits in the bitstream.

The next and slightly more complicated step is use the parameters of the wavelength, core radius, and refractive indices to calculate the *V-number* and use a function for calculating the zeros of $J_\nu(x)$ to calculate how many modes of azimuthal order ν can and will be stimulated. We express the *V-number* as

$$V = \frac{2\pi}{\lambda}\sqrt{n_c^2 - n_{cl}^2} \tag{1.4}$$

This number describes the range of allowed modes in an optical fiber. The largest value for ν, the azimuthal index number, is $2V/\pi$ [14]. More specifically, the mode allowed is dependent on its value in relation to the *n*th zero of a Bessel function of the first kind of order ν

as demonstrated in Figure 1.3 below. Figure 1.3 illustrates this principle in the larger context of an *N*-mode MMF. This is more specifically related to the stimulation HE and EH hybrid modes through the weakly-guiding approximation this concept can be extended to LP mode groups. This becomes slightly more complicated given that—at least for short-haul fibers—we are using LP modes for our units of modal stimulation. This method is used to create a filter bank of modes for the optical correlation.

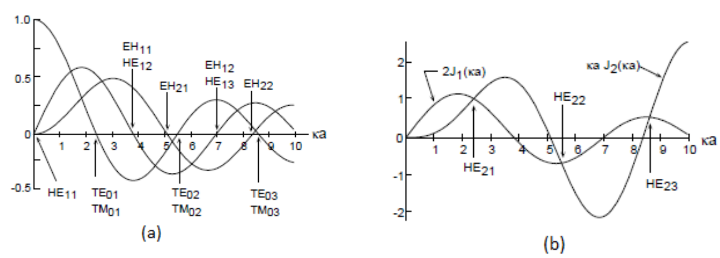

Figure 1.3: The first three Bessel functions of the first kind are plotted with respect to where V or κa intersects with their respective roots [14].

The cutoff conditions for the modes in the fiber are described thusly:

$$TE_{0m} \text{ modes } \leftrightarrow V > m^{th} \text{ root of } J_0(V) \tag{1.5}$$

$$TM_{0m} \text{ modes } \leftrightarrow V > m^{th} \text{ root of } J_1(V) \tag{1.6}$$

$$EH_{\nu m} \text{ modes } \leftrightarrow V > m^{th} \text{ root of } J_m(V) \tag{1.7}$$

$$HE_{\nu m} \text{ modes } \leftrightarrow V > m^{th} \text{ root of } \left(\frac{\varepsilon_c}{\varepsilon_{cl}} + 1\right) J_{\nu-1}(V) - \frac{V}{\nu - 1} J_\nu(V) = 0 \tag{1.8}$$

In Figure 1.3 (a), we see the EH hybrid modes according to the conditions described in equations (1.5), (1.6), and (1.7). On the right in Figure 1.3 (b) we see the HE hybrid modes according to the conditions described in (1.8). However, because we are using LP modes as our eigenchannels we will have an entirely new set of conditions.

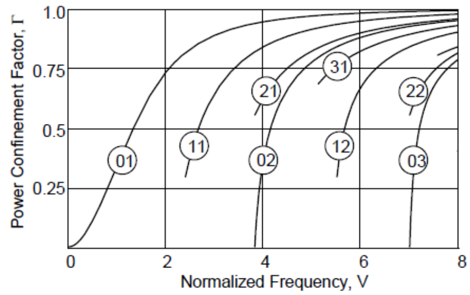

Figure 1.4: The proportional power of $\mathrm{LP}_{\nu m}$ modes carried in the core as a function of the *V-number* [14].

Figure 1.4 describes the new conditions for the excitation and confinement of the LP modes in optical fibers. The designation of the modes is thusly defined by [14]:

$$LP_{1m} = TE_{0m} + TM_{0m} + HE_{2m} \tag{2.11}$$

$$LP_{\nu m} = HE_{\nu+1,m} + EH_{\nu-1,m} \tag{2.12}$$

$$LP_{0m} = HE_{1m} \tag{2.13}$$

Consequently, this model carries a linear combination of variably stimulated eigenmodes through the fiber in such a way as to create a rough approximation of the externally imposed field. This is similar to the way that Fourier series coefficients are generated from an aperiodic signal; in this case the modal decomposition yields something similar to a Fourier-Bessel series. The only difference is that the Fourier modes are orthogonal whereas the fiber optic modes are not, and in fact, oftentimes strongly coupled.

1.4 Optical Fiber as a Communication Apparatus

MMFs can function as robust communication channels as they share many of their properties. For example, they effectively function as filters in radial k-space in that they allow a maximum radial frequency of $k_{max} = k_0$NA [14], where k_0 and NA are the wavenumber $2\pi/\lambda$ and numerical aperture, respectively. Furthermore, the spatial spectrum is discretized into guided modes, corresponding to a discrete set of radial frequencies within the core of the fiber. For this reason, we can model the information externally encoded onto a Gaussian beam pulse as a stimulation of multiple channels.

These "optical channels" propagate in the fiber at different speeds and thus accrue a delay in the process. As is a constant in *all* practical communication systems, the received signal contains additive noise. Noise contaminates the spatiotemporal amplitude elements of the signal and the phase of the signal. In the fiber, this happens by way of successive wavefronts contaminating the mode. From a spatial perspective, this is noise that contaminates the intensity field of the optical mode. Additionally, dark current and shot noise enter the signal at the receiver. The signal-contamination by these various noise sources will be modeled as additive white Gaussian noise (AWGN).

Competency as a communication system does not just start and end with what happens regarding the optical fiber. The receiver is also a major component of this system as it is the one that is responsible for receiving the signals and appropriately demultiplexing them. This is important to recognize because the thrust of this thesis concerns what happens regarding the *receiver*, not the transmitter (Gaussian beam) or the communication medium (optical fiber). In this way, we can and *do* propose an optical receiver system. Such a receiver must be able to facilitate demultiplexing, be sensitive to relevant encoding, and have a rule-based scheme for sorting signals.

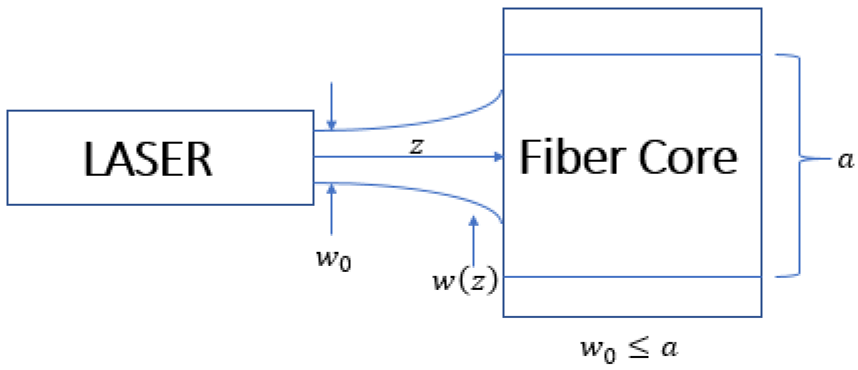

Figure 1.5: The coupling of a parabolically expanding Gaussian beam into a fiber.

Our transmitter will have a beam source at some arbitrary distance directly incident on the fiber. Figure 1.5 is an illustration of how users' input lasers and fiber core couplings, one input beam source per user. We also assume a circularly symmetric beam source, meaning that the modes generated will be various orders of Gaussian-Laguerre modes with curved wavefronts and zero tilted angle. Gaussian-Laguerre fundamental mode of a beam of wavelength λ take the following form

$$E(r,\phi,z) = \frac{E_0 C_{\nu 0}^{LG}}{w(z)} \left(\frac{\sqrt{2}r}{w(z)}\right)^{\nu} e^{-\left(\frac{1}{w^2(z)}+\frac{ik_0}{2R(z)}\right)r^2} L_0^{\nu}\left(\frac{2r^2}{w^2(z)}\right) e^{-i(\nu\phi+kz-\psi(z))} \tag{1.4}$$

where, E_0 is the electric field amplitude, k_0 is the wavenumber, w_0 is the spot size out of the fiber laser, $w(z)$ is the beamwaist as a function of z given by $w_0\sqrt{1+\left(\frac{z}{z_R}\right)^2}$, z_R is the Rayleigh range $\pi w_0^2/\lambda$, the distance from the beam source where the cross sectional area doubles, $R(z)$ is the radius of curvature of the beam as a function of z given by $z\left(1+\left(\frac{z}{z_R}\right)^2\right)$, $\psi(z)$ is the Guoy phase shift as a function of z given by $\psi(z) = (\nu+1)\tan^{-1}\left(\frac{z}{z_R}\right)$, ν is the azimuthal order of the beam, L_m^{ν} is the generalized Laguerre polynomial function, and $C_{\nu 0}^{LG}$ is the normalizing constant to make the cylindrical inner product of the envelope function equal unity $\sqrt{1/\pi\nu}$ [16].

Higher order modes are generally avoided so for the purposes of this thesis the only relevant Gaussian beam modes will be the *radially* fundamental modes, the $\mathrm{TEM}_{\nu 0}$ modes, which stimulate the relevant allowed modes in the fiber. Moreover, this is a few-mode fiber so the azimuthal orders should not get beyond $\nu = 2$. Our purpose is to bypass the issue of azimuthal orthogonality and allow for the LP modes to propagate. Recently, there have been developments in the use of optical elements to generate such modes [17—20]. The problem with these methods is that they do not generate a coherent superposition but rather an azimuthal transformation of the fundamental TEM_{00} mode. Fortunately, methods to generate superpositions of these azimuthal transformations do exist [21].

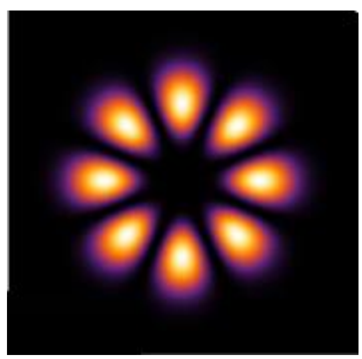

Figure 1.6: Experimental illustration of a Gaussian-Laguerre superposition up to $\nu = 4$ [21].

As shown in Figure 1.6 the superposition of Gaussian-Laguerre produces a “petal” pattern. Additionally, Naidoo et al. in [21] were able to generate such beams with identical losses through the cavity up to order $\nu = 8$. Using this method allows for one to generate LP mode groups where the constitutive modes have equal strength. Here we can develop our own linearly polarized “optical channels” with in the fiber. This would be analogous to the generation of a channel's own system antennas such is the purpose of these beams. This analogy is illustrated in Figure 1.7 on the next page.

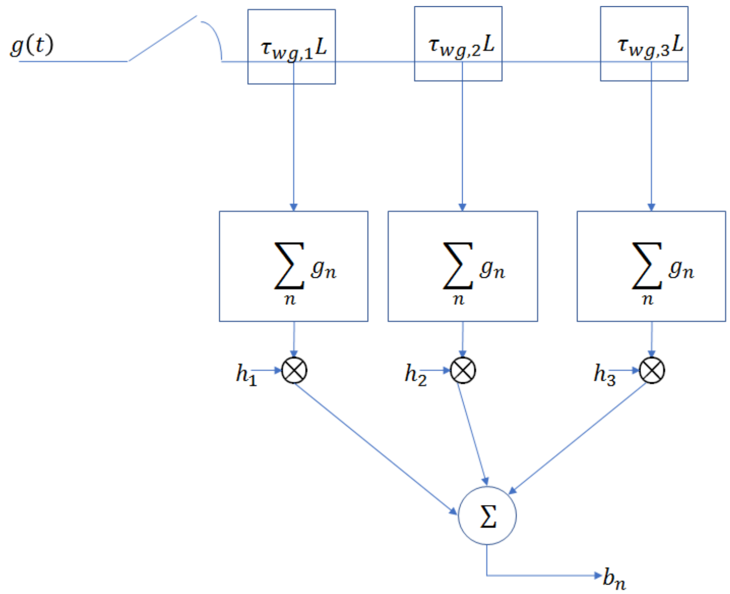

Figure 1.7: The antennas are fed by an information source function $g(t)$ like a multichannel receiver.

The only difference is that radio-frequency (RF) systems allow for the phases and amplitudes to be chosen. Such is not the case for our application of fiber optic modes. The phase information is made irrelevant by our use of direct detection. The amplitudes are functions of the position of the users. On the other hand, the fiber acts as a linear system with an impulse response. Consequently, this means that for some beam that stimulates *K* modes in a fiber of length *L*, this impulse response in time takes the form

$$h_{fiber}(t) = \sum_{k=1}^{K} h_k \delta(t - \tau_{wg,k} L) \tag{1.5}$$

where $\tau_{wg,k}$ represents the waveguide dispersion for the *k*th mode and h_k represents the stimulation amplitudes for the fiber which functions as a multipath channel. For our purposes in this thesis, we will assume a dispersion-compensated fiber where the integrity of the optical pulses is preserved and ISI is thereby eliminated. If this looks familiar it is because it is very similar to the form of the time-invariant multipath impulse response. Here we assume constant amplitudes and the phase factors are absorbed into the coefficients. From here one can characterize channels and come up with a multiplexing scheme that makes use of a source model for single-input-single output (SISO), single-input-multiple output (SIMO), multiple-input-single output (MISO), and multiple-input-multiple output (MIMO) schemes.

In the context of optical design for an optical communications receiver, denoising is an important factor and finding a filter that can do such is important. In this case, the solution is a matched filter. A matched filter works by taking "copies" of a known signal—a template signal—and correlating it with an unknown input signal to measure its presence in a known signal which is our challenge in this work.

1.5 Optimizing Fiber Optic Modal Detection

In the past fiber optic correlation and thus modal detection was done using the analog means of an externally functioning apparatus. This technology was first made available to us in the last half century in the form of the Van der Lugt filter [22]. In this thesis we take advantage of a form of passive analog optical processing of the type described in Figure 1.8.

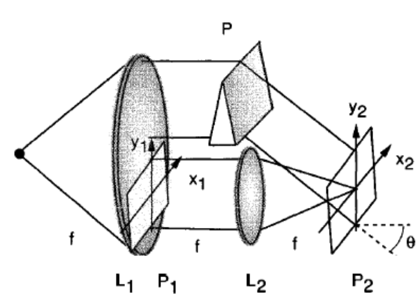

Figure 1.8: Recording the frequency-plane mask for a Van der Lugt filter [22].

The Van der Lugt correlating filter allows one to have a real-time analog optical information processing apparatus for fiber optic modes. The only difference is that those experiments were done with an optical mesh and these are done with photodetector grids. More specifically, we have to find a way of separating the individual modes from the signal at the end of the fiber. Our utilization of FMFs makes this problem much less formidable; indeed these mode selective filters for FMFs have been achieved for two modes [23]. More recently, these methods have been applied for FMFs through *long period grating* mode converters [24]. The more recent method of modal decomposition makes use of optical prisms to separate modes, allowing us to assess not only the system performance, but also the modal performances.

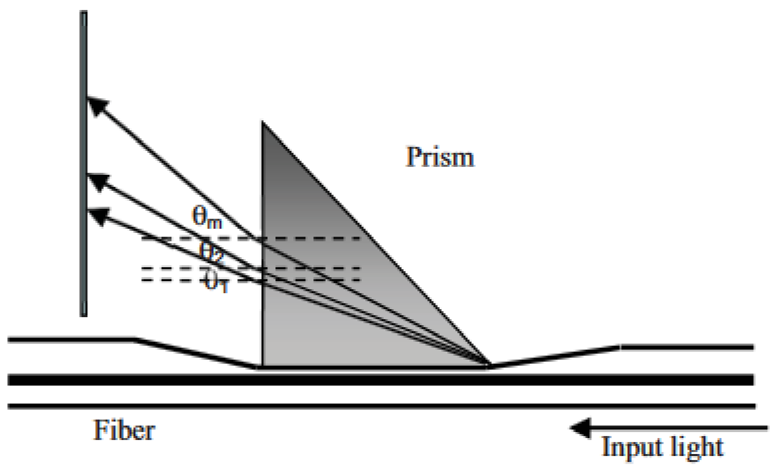

Figure 1.9: Prism attached to side-polished fiber to couple individual modes at different angles, depending on the effective index of the fiber mode [24].

The prism coupler requires a lot of precision to place and can be a source of insertion loss (IL) but it is nevertheless useful for modal separation. The condition to be satisfied here is that the modal separation occurs optimally in the presence of a material where $\frac{(n_p - n_c)}{n_p} \sim \mathcal{O}(10^{-1})$, where n_p is the index of the prism and n_c is the index of the core.

1.6 Thesis Outline

The rest of this thesis is divided into three parts: Chapter 2 will deal with the system model and design that I have proposed, the way it is meant to represent specific conditions of an optical fiber, and an explanation of the how the components are programmatically represented. Chapter 3 will cover the signal processing architecture and various methods involved. Chapter 4 will cover the results of the whole system architecture and make comparisons between various ways of implementing the system.

1.7 Chapter Summary

As of now, typical communication systems are primarily characterized by informational encodings onto variation in signal properties (e.g. frequency, amplitude, phase, etc.); this is known as modulation. Furthermore, this modulation is done with a keying scheme, a scheme that establishes different types of modulation by which this can take place. We provide the necessary context for understanding how multiuser fiber optic systems can function using an FMF and how the current technologies that allow for the success of such a system perform optical correlations in space and time. Also implicated in this work is a few-user model that allows for the generation of user symbols for the n^{th} bit in a bitstream by way of a carefully calculated and optimized detection threshold. This will be further explained in the fourth chapter.

Chapter 2: Optical System Layout

In this chapter we divide our model in to its various components. We first start with our input beam waves from our users that we use to generate the LP mode groups onto which the information is attached. Secondly, the optical fiber is our medium for information transmission. The fiber is the container of the channels and paths that are stimulated therein. Because the users stimulate the same optical channels, there is bit-alignment among users for each channel. There are three ways in which we will test the system performance. One of the ways in which we evaluate the performance of the system is that at the receiver we use a prism for the modal demultiplexing of optical signals. Each of those modes has its own photodiode array for spatial sampling. After which a decision is made among the modes to ascertain the optical symbol generated by the users' bit-alignment.

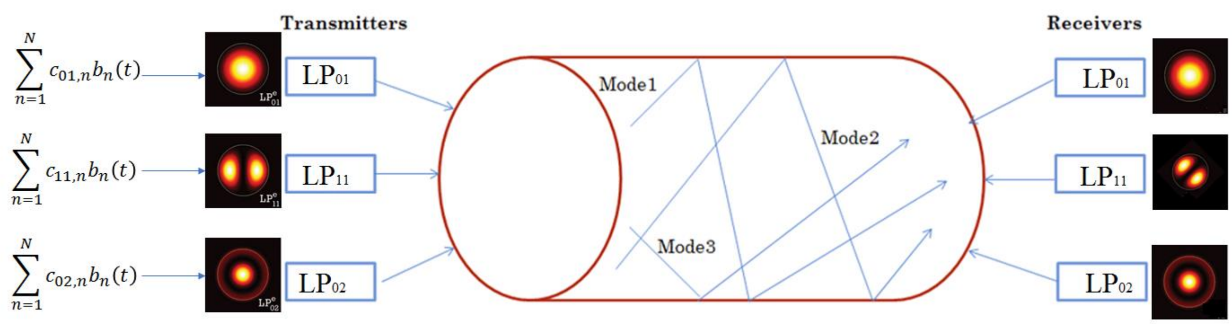

Figure 2.1: An I/O schematic representation of an FMF whose allowable modes are externally stimulated by the users' beams.

The purpose of Figure 2.1 is to provide a more visual intuition as to how the system is mean to operate. For an optical fiber of radius a, we optimize the spot size for the stimulated mode; this standard will change in the next chapters. What we have is an FMF that is stimulated by Gaussian beams which, in turn, stimulate the allowable modes in the fiber.

2.1 Optical Transmission Components

We first start with the "petal beams" generated by our users' fiber lasers to stimulate the allowable modes inside the fiber. This is done through the use of an intra-cavity stop that is meant to generate modes [21]. Additionally, the lasers are differentially positioned at the entrance to the fiber. More will be said about how to optimally position the users for best performance. Suffice it to say that the positioning of the lasers is what defines a user. We take advantage of the channel state information (CSI) to come up with ways to optimize user positions at the entrance of the fiber. This is our linear precoding method wherein our knowledge of the channel's properties allows us to exploit a diversity gain among the users for the minimization of receiver errors.

2.2 Fiber and Channel Components

Starting with the optical fiber, we understand this as a communication channel that carries the channels (modes). We assume that we have the CSI as ascertained by pilot signals. This will be done in single-core and multicore contexts.

We assume a fiber laser operating at a relatively low-intensity, around 1 mW. Additionally, we include the effects of dispersion but not chromatic dispersion. In this way we assume a dispersion-shifted fiber where low attenuation and low-dispersion intersect. In this way, there is delay between the various modes, but the integrity of the pulses is preserved. Such was the case with Cohen et al. using germanium oxide (GeO_2) dopant impurities to make shifts in the refractive indices [26]. This makes our fiber function as a linear system of which we can take the impulse and frequency responses.

2.3 Receiver Components

At the end of the fiber, a prism is used for coupling the modes out of the fiber, demultiplexing them, and sending them into the grid of photodiodes tailored to each mode. For our multicore and single-core contexts there is one prism per core. When placed as close as possible to the fiber core cladding interface(s), such prisms function as low-loss demultiplexers for the modes. Now our spatial sampling apparatus, the microphotodiode array, follows. For simplicity, we will assume that each photodiode has an external quantum efficiency of $\eta_{ext} = 1$. Figure 2.4 shows an approximation of what the sensing array would look like.

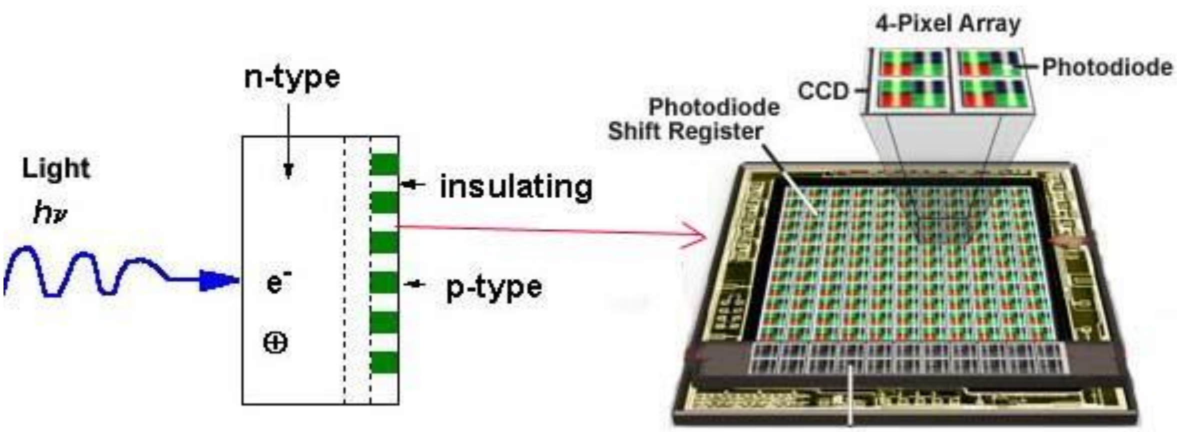

Figure 2.2: The array of semiconductor microphotodiodes how we model spatial sampling [27].

This semiconductor sampling apparatus displayed in Figure 2.2 senses the output signal, then its individual elements perform opto-electronic conversion, inducing a current representation of the signal in each element. For the case of amplitude-shift keying, we use a binary encoding in the form of 1's and 0's. The use of ASK will be relevant for the coding of the amplitude—and thus intensity—of a mode.

Temporally, the small areal dimension of the elements will allow for a fast response time. Experiments specifically with nanophotodiodes have demonstrated a transit time through the depletion layer on the order of picoseconds, evincing a theoretical bandwidth of up to 100 GHz via surface plasmon resonance [28]. These such speeds allow for efficient sampling of each pulse. The intensity of each pixel is detected and an optical "raster image" is created. Each "pixel" entry of the $N \times N$ matrix of the digital mode is described by the equations below:

$$E_{ij} = \frac{1}{(ds)^2} \int_{\frac{2i-N}{2}ds}^{\frac{2(i+1)-N}{2}ds} \int_{\frac{2j-N}{2}ds}^{\frac{2(j+1)-N}{2}ds} E(x,y)dxdy \text{, for } i,j \in [1,N] \tag{2.1}$$

where ds is the side-length dimension of a grid square.

Likewise, the intensity matrix is similarly written

$$I_{ij} = \frac{cn\varepsilon_0}{2(ds)^2} \int_{\frac{2i-N}{2}ds}^{\frac{2(i+1)-N}{2}ds} \int_{\frac{2j-N}{2}ds}^{\frac{2(j+1)-N}{2}ds} |E(x,y)|^2 dxdy \text{, for } i,j \in [1,N] \tag{2.2}$$

where c is the speed of light, ε_0 is permittivity of free-space, and

$$n = \begin{cases} n_c, & x^2 + y^2 < a \\ n_{cl}, & \text{else} \end{cases}$$

where n_c and n_{cl} are the respective core and cladding indices.

At the end a type of decision algorithm is used to match the information to its respective mode. This model will become more complex as we progress through this work but suffice it to say that this is only a rough sketch.

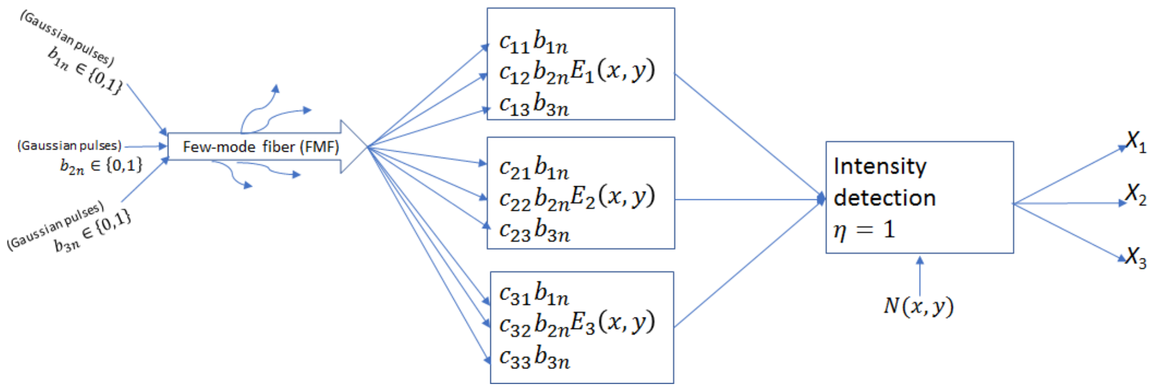

Figure 2.3: The elementary fiber system model.

In Figure 2.3, b_{mn} is the n^{th} bit of the m^{th} user, c_{lm} is the excitation of mode l by user m, $N(x, y)$ is the two-dimensional AWGN component, and X_m is the decision of the m^{th} mode. In this there are two ways in which this thesis will model noise. The purpose of a matched filter is to maximize the SNR of a signal in the presence of AWGN. We rely on linear systems to ascertain the matched filter. One should keep in mind that is this the temporal one-dimensional case. Our examination of the two-dimensional case is further ahead. In this case our goal is to come up with an impulse response meant to maximize the value of $x(t) * h(t)$ at an arbitrary time. Our temporal pulses in this case are Gaussian pulses centered at $t = T_b/2$, where T_b is the bit period. Because our pulses symmetric about $t = T_b/2$ the temporal "integrate and dump" correlator is a close approximation a matched filter [29].

The system works by using maximum-likelihood (ML) estimation to measure the correlations of the spatially sampled optical LP modes with mode templates. The method works by first a using a spatially sampled representation of one of the modes stimulated by the Gaussian input beam and loading up the bits (1 and 0) where both are equiprobable. In the context of direct detection, it is not sufficient to use the sign of the bit decision. Instead, we take a weighted sum of the users according to their respective excitation amplitudes. The correlation between the LP modes is not only supposed to function a modal classifier, but also used to give us a symbol energy for the particular user-symbol sent. This is something that is done while each pulse is temporally sampled.

2.4 Optical Modal Correlation and Filtering

In applying optical detectors for spatial matched filtering, one must still apply the mathematical methods used for a temporal matched filter. After spatial sampling and temporal correlation, the modal energies are calculated compared to a theoretical value in a bank of spatially sampled representations of modes. Our purpose here is finding the relative correlation—covariance more precisely—between each mode, choosing the highest, and using ML estimation on those values.

In this model, we propose a stream of Gaussian pulses in time of the form

$$p(t) = P_0 e^{-4\ln 2\left(\frac{t}{\tau_p}\right)^2} \tag{2.3}$$

where τ_p is the FWHM pulse duration and P_0 is the power of the pulse at $t = 0$. Since we are using noncoherent detection, we will be using power pulses rather than field pulses. The frequency spectrum of $p(t)$ is expressed as

$$\tilde{p}(\omega) \propto e^{-\frac{\omega^2\tau_p^2}{16\ln 2}} \tag{2.4}$$

Using the FWHM rule on the frequency spectrum, we get that the 3 dB frequency and 3 dB bandwidth are

$$f_{3\mathrm{dB}} = \frac{\ln 4}{\pi\tau_p} \leftrightarrow \mathrm{BW} = \frac{2\ln 4}{\pi\tau_p} = \frac{0.88}{\tau_p} \tag{2.5}$$

Using the Nyquist-Shannon sampling theorem for which $f_s > 2\mathrm{BW}$, we conclude that the required sampling rate must be at least $1.76\tau_p^{-1}$, corresponding to a minimum of two samples per pulse—within the FWHM pulse duration. In this way, the model has the bitstream essentially "interleaved with itself"—creating double copies of each bit—in order to capture the double sampling aspect of the model. However, this is not enough to robustly capture the temporal aspect that requires the "integrate and dump" calculation process or a robust temporal correlation process. In short, we need a more rigorous definition of our signal bandwidth, one that matches how we define the pulse duration in the time domain.

2.5 Chapter Summary

In this chapter we have broken down the computational system components to get a more programmatic picture of how this system will be realized. We described this entire I/O model system from start to end. From the transmitter we have demonstrated the ability to stimulate modal superposition of Gaussian-Laguerre modes without a cumbersome integration of optical elements [21]. We also have a mathematical channel model for the fiber in terms of how it there are multiple paths with different delays over the course of the component. We have ignored the effects of chromatic dispersion, having demonstrated they can be accounted for through doping while simultaneously exhibiting low fiber attenuation [26]. Our prism coupler is our demultiplexer, allowing for a separation of modes for an individual correlation to the noiseless eigenmodes. These modes are pre-stored as matrices, "stored" in the detector for all intents and purposes. The temporal component enters as relevant sampler samples at least twice—most likely more—per bit. Altogether we will have a representation of the matched filter correlator in the x, y, and t domains.

Integrating in time is how bits are *temporally* separated; the bits are correlated with a "high" Gaussian pulse. In essence, we basically have an optical multipath receiver for a selected ensemble of users in the context of an OOK modulation scheme. Information is fed through the eigenchannels (modes), giving us a point of connection with a typical electrical communication system. The communication channel allows for us to build a matched filter for each channel. As the users stimulate the same modes, the modes thus carry the same information. However, the question remains as to how to optimally extract this information.

Chapter 3: Signal Processing for Fiber Model

In this chapter, we discuss how signal processing is done at the level of the receiver. We take from A.P.T. Lau's model in [22] and use direct detection for the microphotodiode grid receiver. In this way the bit stream conglomerate is modeled as

$$E(r,\theta,z=0,t) = e^{j\omega t}\sum_{m=1}^{M}\sum_{n=1}^{N} b_n(t)c_{mn}\,E_m(r,\theta,t-mT_b-\tau_m)e^{-j\beta_m z} \tag{3.1}$$

where, $b_n(t) \in \{0,1\}$ is the OOK bit stream of the *k*th bit, β_m is the wavevector for the *m*th mode, ω is the optical frequency, τ_m is the waveguide delay for the *m*th mode, and T_b is the bit period. In this scheme, noise is added to the *intensity* of the received mode such that the signal received in a fiber of length L is expressed as

$$|E(r,\phi,t)|^2 = \sum_{k=1}^{K} b_k^2|\psi_k(r,\phi,t)|^2 + \underbrace{2\sum_{i\neq j}^{K} b_i b_j \psi_i(r,\phi,t)\psi_j(r,\phi,t)\cos(\beta_i-\beta_j)L}_{\text{cross-terms}} + \underbrace{N(r,\phi,t)}_{\text{noise}} \tag{3.2}$$

In the previous chapter, we noted how operations of integration were reduced to operations of addition through spatial sampling. While this is good for the direct terms of the mode intensity when one is trying to make correlations with modally matched filter banks, this sort of process becomes more difficult in the realm of cross terms. These cross terms come from the differences in the β for certain modes. However, in our model, they will arise from the phase differences of the excitation amplitudes for the few LP modes generated by the Gaussian beam. Under the weakly-guiding approximation, the value of β takes the form described by Davis in [2] and A. Juarez [31] as

$$\beta_{\nu m} = n_c k_0 \sqrt{1 - \frac{2\sqrt{2\Delta}}{n_c k_0 a}(2\nu + 2m + 1)} \tag{3.3}$$

where, n_c is the core index, k_0 is the k-vector, a is the fiber radius, Δ is the relative index difference, and ν and *m* are the azimuthal and radial indices, respectively.

Additionally, these beams are assigned to each of the few users. The square power law makes it such that a cross term also become carriers of information. This problem becomes more difficult in the context of a large mode fiber [32], which is why our model only deals with FMFs. This mixing, which is often very high can often make it hard to distinguish one cross term from another; this is one of the consequences of user interference. This is especially true if the modes being used are linearly polarized approximations to hybrid modes stimulated in the fiber. Since LP modes are really superpositions of two—sometimes three—hybrid modes, the cross terms could contain four—or even *eight*—cross-terms. However, the length of fiber we use for our model is more short-haul and so the effects of this sort of dispersion can be ignored. The effects of extreme delay that would cause the modal separation will not play a major role this model. The model proposed is one that attempts to solve issues related to user interference in the presence of noise by proposing ways of implementing this system in already existing communications schemes.

3.1 Optimizing Receiver Architecture

One would think that an advantage is offered by a concentric array which not only matches the geometric structure of the fiber, but also consequently allows for fewer samples to be taken as the only the radial component is important due to the azimuthal symmetry. The same cannot be said of higher order axial modes.

The lack of an azimuthal sensor means that polar sampling—sampling in r and ϕ—cannot take place in an FMF. Additionally, this means that the spatial spectrum of modes cannot be holistically examined. Additionally, since we are encoding the information onto LP mode groups then the same information would be time shifted by temporal samples. This would lead to information mixing and a different information that would effectively come from a different user.

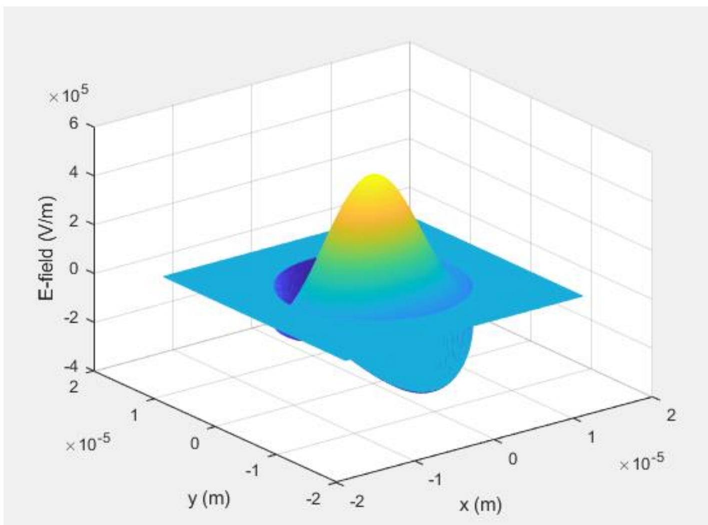

Figure 3.1: A cross-sectional model of the LP_{12} mode field in an optical fiber.

The LP_{12} mode field shown in Figure 3.1 is plotted as a superposition of TE_{02}, TM_{02}, and HE_{22} modes, which are degenerate as they travel roughly at the same speed. The reliability of our ability to collapse the modes into one is ensured by the fact that a 632.8nm wavelength with an NA of 0.0548 has an intramodal time-shift of only 188 ps for every 1000 km. Because the modes have two *different* azimuthal components—components in the ϕ-direction—they are essentially orthogonal but nevertheless degenerate. Consequently, looking at their Hankel transforms will not be effective because their azimuthal numbers are not the same. Spectral analysis is not an option for us with an FMF as concentric rings cannot capture the azimuthal component beyond the fundamental mode. It is for this reason that we *must* use grid Cartesian rectangular photodiode arrays because they are compatible with a more holistic sampling of a mode's cross-section. This is especially true when existence of user interference comes into play. A cross term of a "1" on both the LP_{12} and the fundamental radial mode is demonstrated in Figure 3.2.

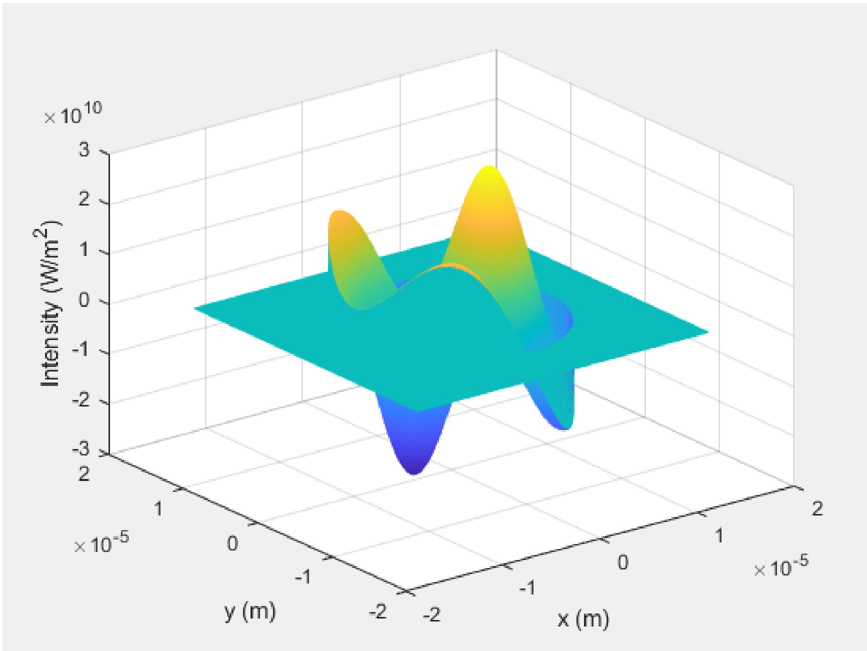

Figure 3.2: The LP_{12} and LP_{01} mode field are plotted together as a cross-term.

Taking the modes as one stream and incorporating it into a fiber would be difficult in terms of algorithmic demultiplexing. For this reason, our model bypasses the modal cross-terms such as those that would appear in Figure 3.2.

We further demonstrate that such a system can be extrapolated from theoretical conditions as we make a variation of a channel segmentation model formulated by Juarez et al in [31] that was used to model fiber bending. Instead, our variation models index perturbations in both the core and cladding wherein the velocity of each mode varies according to its fiber segment. We use a variant of Juarez's channel model, also used by Davis used in [2], with a Gaussian distributed in index variation where both n_c' and n_{cl}'—which are the respective new indices of the core and cladding—were distributed as $n_c' \sim \mathcal{N}(n_c, \Delta n^2/100)$ and as $n_{cl}' \sim N(n_{cl}, \Delta n^2/100)$, where $\Delta n = n_c - n_{cl}$. Figure 3.3 below shows the delay of the constitutive modes of the LP_{12} mode group as a function of the number of divisions.

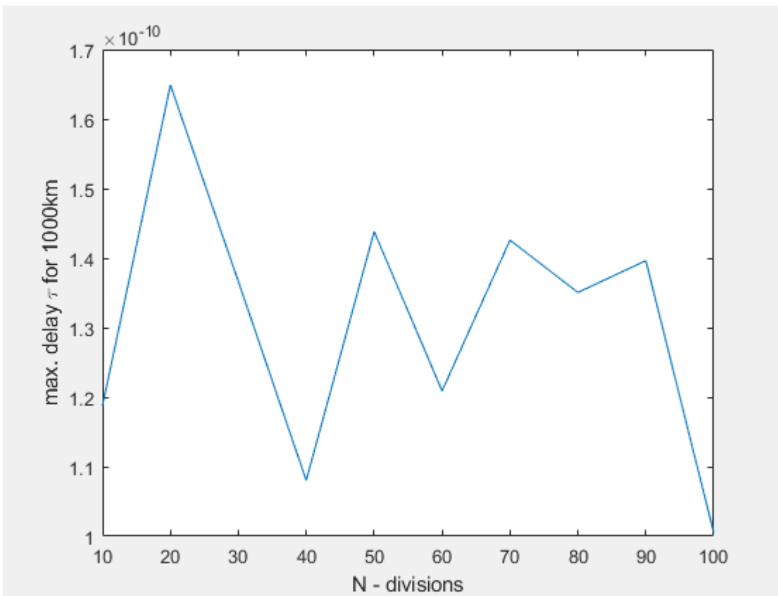

Figure 3.3: The total delay the among the constitutive modes of the LP_{12} mode group over the course of 1000 km.

In Figure 3.3 we observe that the delay remains on the order of 10^{-10} seconds for 1000km which represents a phenomenally small delay between the already degenerate radial modes—TE_{02} and TM_{02}—and the HE_{22} axial mode. The delay τ in Figure 3.3 reaches a minimum low of .10 ns for 1000km when there are 100 segments, 10 km per segment. Overall, the value of τ decreases as the number of segments increases. This can likely be attributed to a form of the law of large numbers where a mean of some sort is approached as the number of iterations increases. We our system makes use of a short link of only 25 km, making our delay on the order of .1% of our bit rate, on the order of picoseconds (10^{-12} seconds), a time scale too short to affect diode temporal sampling. With a bit rate of 1 Gbps, our system does not suffer from the long-haul intramodal delay.

There is one purpose served by the taking the Hankel transforms, the radial spectra, of the modes and that is to come up with an idea of the sampling frequency in space. This is done through the Hankel transform [33] expressed in (3.4) as

$$E_\nu(k) = A\int_0^a J_\nu(\kappa r)J_\nu(kr)r\cdot dr + C\int_a^\infty K_\nu(\gamma r)J_\nu(kr)r\cdot dr \tag{3.4}$$

where ν is the azimuthal number and A and C are the boundary coefficients for the core and cladding, respectively. The corresponding transforms is plotted for the radial component of HE_{21} mode intensity.

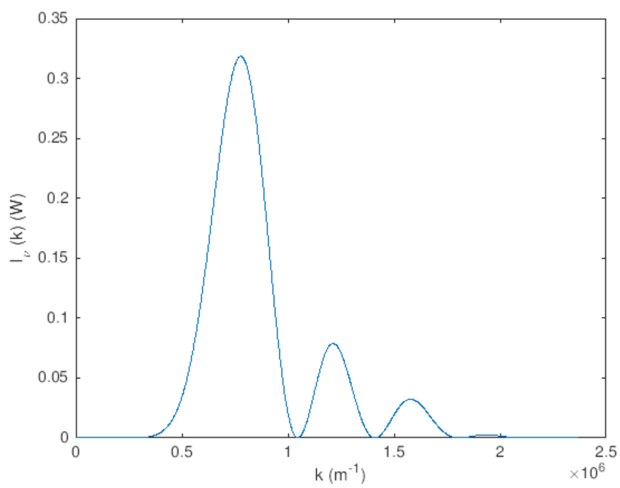

Figure 3.4: The power spectral density (PSD) of the HE_{21} mode intensity field in radial *k*-space.

For our sensing applications, there is not much to be gleaned from the Hankel transform in Figure 3.4 except for an understanding of what the approximate radial bandwidth would be.—$\mathrm{BW}_k \approx 3.455\cdot 10^6\ \mathrm{rad}\cdot\mathrm{m}^{-1}$; the bandwidth is $1.7275\cdot 10^{-6}\ \mathrm{rad}\cdot\mathrm{m}^{-1}$ in positive *k*-space but we double it as $E_\nu(k)$ is even with respect to k. Because k is the angular spatial frequency in radial k-space, we can express k as $k = \sqrt{k_x^2 + k_y^2}$ where $\min k = 2\mathrm{BW}_k$ and $\min k = 6.911 \cdot 10^6\ \mathrm{rad} \cdot \mathrm{m}^{-1}$. Consequently, both k_x and k_y must have a minimum of $2\mathrm{BW}$ to account for the whole circle. After dividing by 2π to get $\min \xi_x$ and $\min \xi_y$ we take their reciprocals to give us $\lambda_x = \lambda_y = 0.91$ µm. Our appeal to cylindrical transforms is for an illustrative understanding of how to use Nyquist's theorem in cylindrical space and then subsequently apply it to Cartesian microphotodiode sampling.

3.2 Temporal Processing

In the previous section we discussed intramodal separation in the context of long-haul fibers. Our spatiotemporal hybrid correlator can ameliorate this problem. The orthogonality in space can be rectified by taking advantage of the connection these pulses have in time. The robust temporal sampling allows us to incorporate the pulse delay between two degenerate modes *into* our spatiotemporal correlator such that there is effectively zero delay. The temporal processing component works as a corrective to the degradation of LP modes over long distances. More precisely put, an LP mode is modulated with a single Gaussian pulse is mathematically expressed by

$$E_1(x, y, t) = E_{1a}(x, y)e^{-2\ln 2\left(\frac{t}{\tau_p}\right)^2} + E_{1b}(x, y)e^{-2\ln 2\left(\frac{t-\Delta\tau}{\tau_p}\right)^2} \tag{3.5}$$

where $E_1(x, y)$ is the optical field of the LP mode, $E_{1a}(x, y)$ and $E_{1b}(x, y)$ are the two degenerate components, and $\Delta\tau$ is the time delay between the modes. Robust temporal sampling allows for the connection in time to be seized upon in order to skirt the problem of degeneracy degradation over long distances for LP modes.

The mathematics of the temporal processing of the bit stream was described in the previous chapter but is important to note that the sampling of Gaussian pulses will also occur. Fortunately for us, the Gaussian pulse only acts as a temporal coefficient for the spatial profile. Altogether, the bitstream can and does function as such a coefficient, varying in time as it modulates the spatial profile of the mode such that $E_i(x,y,t) = \sum_k c_k b_k(t) \cdot \psi_i(x,y)$. This means that we will repeatedly sample the incoming beam in order to fully capture a bit. The form that the Gaussian pulse *at the end of the fiber* takes is

$$P(t) = P_0 e^{-\alpha L} e^{-4\ln 2\left(\frac{t}{\tau_p}\right)^2} \tag{3.6}$$

where $\alpha$is the attenuation coefficient for the fiber and L is the length of the fiber. Integrating the pulse over all time gives us a pulse energy of $E_p = \frac{P_0 e^{-\alpha L} \tau_p}{2} \sqrt{\frac{\pi}{\ln 2}}$. Most of the signal—98 percent—will be captured in the interval $[-\tau_p, \tau_p]$. If we sample at a rate T_s, then we can take basic Riemann sums of the pulse in *time* as effective integration. However, given that we are making use of a spatial-temporal paradigm, we use a temporal correlator. For our purposes this takes the form of a Gaussian "dummy pulse" that is matched to the specifications that constitute one "high" bit. The Nyquist requirement approximated in the previous chapter is a mere benchmark for how real-time temporal sampling should take place. This would involve allocating a certain number of samples per pulse or bit which would then work in combination with spatial correlator in that it would integrate the power received of the mode's spatial profile *in time* and then then scale that power according to which portion of the Gaussian pulse was simultaneously sampled.

We showed in Chapter 2 that 98 percent of the Gaussian pulse energy is captured from $\left[-\tau_p, \tau_p\right]$ as the pulse takes the form $p(t) \propto e^{-4\ln 2\left(\frac{t}{\tau_p}\right)^2}$. We made $\tau_p = 0.4T_b$ for the purposes of approximating an ideal model with some ISI, which was the larger motivating factor in approximating the Gaussian bandwidth in a different way. In order to capture the equivalent amount of energy in the frequency spectrum we would have to make $\frac{{\omega^*}^2\tau_p^2}{16\ln 2} = 4\ln 2$. We come up with a bandwidth of $\mathrm{BW} = 2\omega^* = \frac{16\ln 2}{\tau_p}$ and a necessary condition that

$$\omega_s \geq \frac{32\ln 2}{\tau_p} \leftrightarrow f_s \geq \frac{16\ln 2}{\pi\tau_p} \tag{3.7}$$

In a pulse range of length $2\tau_p$ there *must* be at least $\lceil 32\ln 2/\pi \rceil$, or 9, samples per pulse necessary for rigorous sampling within this range, where $\lceil\cdot\rceil$ is the ceiling function. For good measure, our sampling rate was $f_s = 10T_p$, where T_p our Gaussian pulse length in the context of our Gaussian pulse amplitude modulation (PAM) scheme.

The spatial-temporal architecture provides two—or three if you include cross-terms—degrees of confirmation for what is being sent and received. So far what has been done here is single-input-single-output (SISO). This is to say that we have been dealing with only one mode at a time and encoding formation onto said mode and looking at the end result; we have not yet sampled a pulse train of bits.

This architecture can be generalized to a multiple-input-multiple-output (MIMO) system but complexity sharply increases in doing so and our work here is with an FMF. Accordingly, we can compromise and instead work with a FIFO (few-input-few-output) system, not to be confused with the "first-in, first-out" method from network and computing theory. With this compromise we can have a more complex challenge regarding how this system would work for multiple users instead of one. But we are additionally challenged out to optimize user settings for information recovery. However, comparisons will later be made to multicore system with multiple SMF cores.

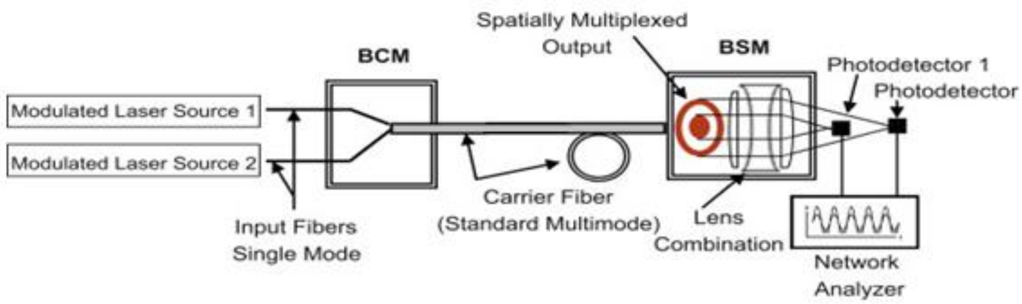

Figure 3.5: The block diagram above shows the basic FIFO architecture with two inputs that are spatially demultiplexed by the same number of outputs [34].

We consider the architecture in Figure 3.5 with a few exceptions. Here we will be matching photodetectors arrays to "store" the noiseless pulsed modes "reference modal pulses" much similar to how the Van der Lugt filter used a reference in its analog application of the same process.

To reiterate, our model was built and tested in chunks: first working correlator and then the grid array for the reference mode. However, noise is inevitably added in this system by way of the detector; this is what will constitute the spatial and temporal noise. This is to say that $E(x, y, t) \rightarrow E(x, y, t) + N(x, y, t)$, where $E(x, y, t)$ is the bitstream-modulated electric field and $N(x, y, t)$ is the added noise.

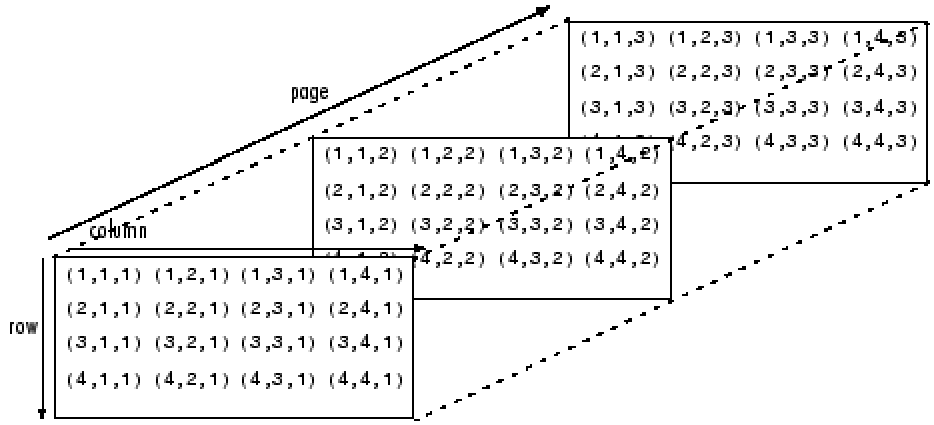

Figure 3.6: The profiles are modeled as a succession of grid arrays that evenly sample the electric field and intensity.

Figure 3.6 is a representation of the spatiotemporal bitstream. The rows, columns, and pages represent the *x*, *y*, and *t* axes. This programmatic representation is how our information is represented in the MATLAB simulation.

3.3 Realizing FIFO

Multiple-input-multiple-output (MIMO) only complicates things for our model as the number of correlating filters needed rapidly multiplies and the amount of modal mixing increases as well and the demultiplexing process becomes more complex. For now, this problem can simply be reduced by use of FIFO in the context of a short-haul fiber. However, similar issues with multiplexing still arise as the same modes are stimulated with different bit-streams. From few-user input comes few-level detection as one can recall from Section 1.3 that the modes are stimulated by a Gaussian-Laguerre beam. In the context of direct detection this means that the power of a mode stimulated by a user will be proportional to $|c_{\nu m}|^2$. In the context of OOK modulation, this gives a few levels by which one can distinguish a few users. Additionally, using differential modal stimulation allows us to perform an analysis of the systems proficiency as seen by the users instead of the modes.

These levels arise from the alignment-dependent excitation amplitudes that give us a certain detection threshold for each user. In this model we assume the lasers are touching the fiber core entrance. Since we are dealing with FMFs, our predominant focus will be the excitation of lower order LP and hybrid modes with regards to user-specific offsets as described in [35]. In the application of the full system, the modes propagate simultaneously, but they are also superpositions of the bitstreams.

We first go about this under the assumption of coupled users in an SCF. For example, if a given mode ψ_m has an intensity stimulation amplitude of c_m and there are M users and thus M bitstreams, then the value energy for the *n*th bit is described by

$$h[nT_b] = \left|\sum_{m=1}^{M} b_{m,n} c_m\right|^2 \tag{3.10}$$

Furthermore, if we are using simple binary ASK, then the number of decision levels to distinguish becomes 2^M. Therein lies the main problem with implementing massive MIMO communication on a relatively simple and accurate method for SDM and MDM. What is worse is when certain sums of c_m become almost indistinguishable, the susceptibility to errors increases massively such that a *very* high SNR is required to get remotely accurate processing.

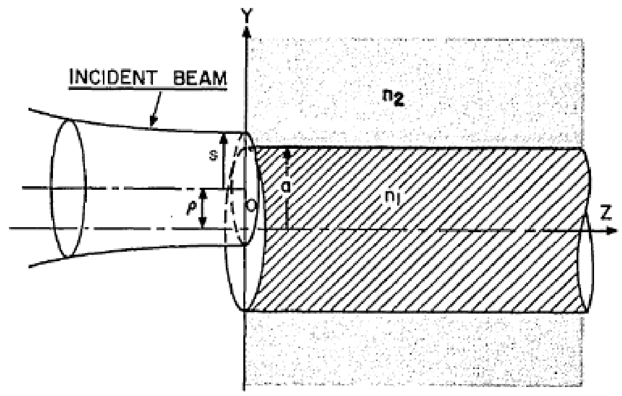

Figure 3.7: A geometric configuration of the beam profile at the fiber input where s is the beam waist at the entrance to the fiber and ρ is the beam offset [35].

The stimulation is something that varies with the offset described in Figure 3.7. The lasers of each user all have certain stimulation coefficients. This is one of two models for how the user will be represented at the beginning of the fiber. The other model will involve a multicore fiber (MCF) wherein there is one user per core. Here, there is one input laser per user and one matched filter per mode. Additionally, the matched filters are temporally matched to the relative delay of a mode.

Our next step is to optimize the spot-size of the laser for each mode in fiber. Here we choose the spot-size w_0 to minimize the amount of insertion loss (IL) for each of the stimulate modes of the fiber.

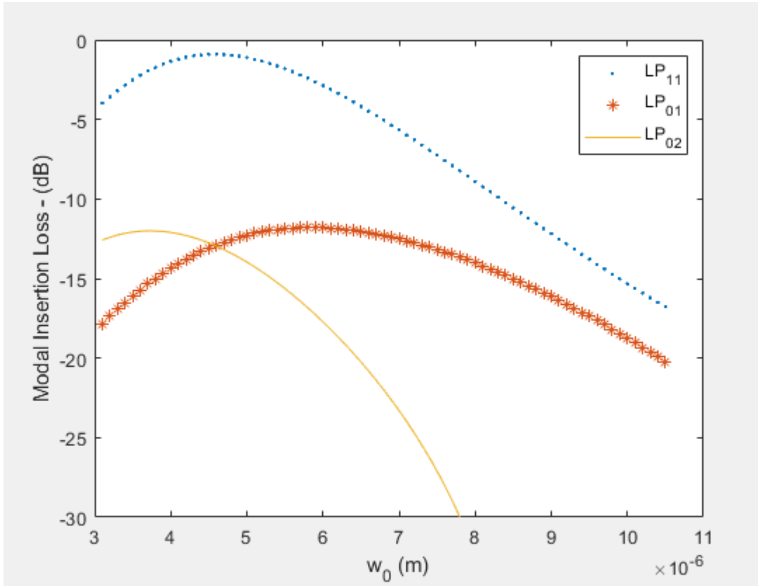

Figure 3.8: A plot of the modal IL in our FMF as a function of the spot-size w_0 of our input Gaussian-Laguerre beam.

Our test case in this regard is detailed in Figure 3.8 in that we hypothesize a Gaussian-Laguerre beam and its ability to stimulate modes with zero radial offset. Here we neglect the effects of reflection for the air-SiO_2 interface. We use a spot-size of $w_0 = 4.6$ µm. In this way the two higher order modes, the LP_{01} and the LP_{02}, have the same level of stimulation at the fiber origin which corresponds to an IL of 12.9 dB. At this spot-size the IL for the LP_{11} mode is 0.904 dB at the same point.

3.4 Multiuser System Optimization

Because the LP_{02} and LP_{01} both have the same level of stimulation, the two modes become the limiting modes. The peak of stimulation occurs at the center, $\rho = 0$ µm, where ρ is beam-offset, which is our test case for Figure 3.8. However, a calculus of sort needs to be done on the proper user arrangement that ensures that enough stimulation is occurring for user distinctions in the presence of noise and that the users have different excitation coefficients to avoid getting functionally degenerate user-symbols. At the receiver there must be a multiuser sorting algorithm for the energies of the symbols received. The sorting is done by use of user-symbols that combine the *n*th bit of *all* the users into one single code, a symbol corresponding to the *n*th bit of the different users. In this way all the gain values c_n must be different to avoid degenerate symbols that are indistinguishable. One could fix this problem by establishing an operational SNR around which we can expect the system to operate, a *design* SNR—SNR_d. However, we can actually bypass the creation of a design parameter altogether as our purpose is to maximize the smallest energy ratio between user-symbols. This helps us maximize the minimum distance between constellation points.

The purpose here is to ensure that there is little to no room for noise corruption to create symbol degeneracy. In trying to diagnose our errors with this method, we eventually learned that symbol errors were likely due to weak-stimulation offsets that resulted in a form of suppression wherein the strength of a user in the system was less than that of other users. Additionally, this helps because the energy/power ratios that are represented in dB allow one to optimize for the highest noise-energy buffer zone among all possible users.

In our model we will use three users. Consequently, there are three users we know that there will exist eight possible codes as per the previous section. An energy threshold is matched to each code combination of the bit streams. The users excite the same modes in the fiber and thus create bit alignment for each mode. Upon being received we can sum these modes together to give us an energy received by the photodetector grid. We then use our look-up table (LUT) for minimum-distance estimation to mathematically calculate the bit codes. The different degrees of modal excitation allow for distinctions to be made between user symbols, thus simplifying the operation of users.

For each mode, the received data can be sorted according to the corresponding binary code to which the energy level matches. These are called user symbols. In the case of 3 users at the n^{th} bit, if user 1 has a '1', user 2 a '1', and user 3 a '0', the corresponding user symbol is $\underline{x} = \underbrace{(1\ 1\ 0)^T}$. It is also worth noting that the system is order-sensitive; that is, it can detect the difference between $\underline{x} = \underbrace{(1\ 1\ 0)^T}$ and $\underline{x} = \underbrace{(0\ 1\ 1)^T}$ as different bit positions have different weights due to the stimulation coefficients. For a particular LP mode, the users are bit-aligned and the overall system is a few-input-single-output (FISO) system with respect to the *users* attached to a certain mode. This user symbol is received as energy corresponding to its value in in a look-up table (LUT). The value in the LUT is then stored as a binary value as its components are split up into three parts, each bit corresponding to the output for each user. The purpose is to find the which arrangement's smallest symbol energy ratio is the largest among all the possible look-up tables that will be generated for multiuser detection. More generally, we express this as

$$(\rho_i^*, \rho_j^*, \rho_k^*) = \underset{i,j,k}{\max} \min\left|u_m(\rho_i, \rho_j, \rho_k) \oslash u_m(\rho_i, \rho_j, \rho_k)\right| \text{ for } i \neq j \neq k, \forall m \tag{3.11}$$

where ρ_k represents the *k*th slot (offset) for a particular user, $u_m(\rho_i, \rho_j, \rho_k)$ is the LUT for the *m*th mode, and $\oslash$ denotes the element-wise division of the LUT.

For our purposes, in our simulations there were 21 radial offset positions per user; these are input laser offsets for the users to stimulate the modes in varying degrees. They are separated by $a/20$ or 0.5 µm, giving us 21^3, or 9261 possible combinations. We run through every single user's arrangements by making a base-21 numbering system for each the users. Our results are shown in the following table:

Table 3.1: Optimized User Offsets for System Performance

User	**Offset (μm)**
1	± 2.5
2	± 5.5
3	± 8.5

3.5 Chapter Summary

The signal processing done here is one that considers the spatial aspect of the signals and how to exploit signal properties for faster transmission. Additionally, the signal processing methods we use when exploiting these properties of the signal are less computationally taxing. Much more will be said about this in the next chapter. In this chapter, we presented a method of optimal matched filtering and correlation, diagnosed the errors that would occur in a case of multiuser detection, and found a way to optimize the user-offsets for best all-around performance. The next chapter will present the results of this multiuser system according to our established parameters and make comparisons across different ways of informational encoding.

Chapter 4: Results and Conclusions

Now that we have the various modules in place, we can come up with an ideal few-user model with specific parameters. Here we used the typical standard wavelength of $\lambda = 1550$ nm for all three users as it has the lowest fiber absorption over long distances. In the context of an FMF, we use the weakly-guided mode approximation where the relative index difference Δ is very small, where $\Delta = (n_c - n_{cl})/n_c$. The fiber core radius a is 10μm and consequently the normalized propagation frequency number V is small enough as to accomodate only a few modes; in this case three.

With our model, the users are randomly assigned various radial offsets in the *y*-direction denoted as ρ_n. We first evaluate an independent uniform assignment were each spot is distributed as $\rho \sim \mathcal{U}(0, a)$—a stochastic assignment of users. In the previous section we already ascertained the optimal combination of users. However, we explore further how sensitive the results are to the initial offset conditions of the users. On the receiver side we will investigate the effect of spatial sampling on the BER, specifically where the BER goes into diminishing returns with increasing grid size. As our square grid has dimension of $3a \times 3a$, where $a = 10$ μm, and we will deal with a 33×33 grid with a linear grid dimension of $ds = 0.91$ μm.. These will be done in parallel with the temporal sampler that builds its own array of bits based on the sampling of Gaussian pulses.

4.1 Spatiotemporal On-off keying (OOK)

Figure 4.1 illustrates the constellation diagram of the spatiotemporal OOK modulation, at the output of match filter introduced in for the LP_{12} mode by a helium-neon beam given the aforementioned core radius where $\lambda = 632.8$ nm and $\mathrm{NA} = 0.122$.

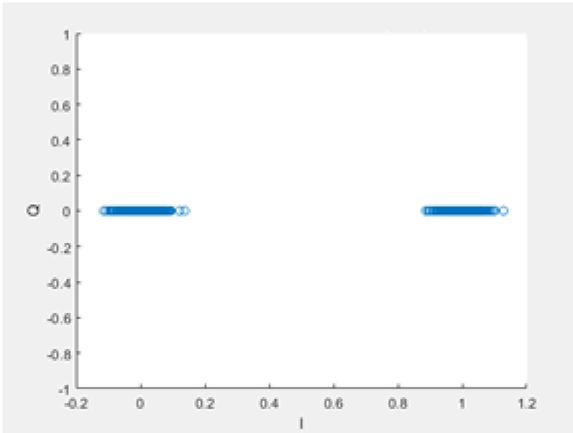

(a)

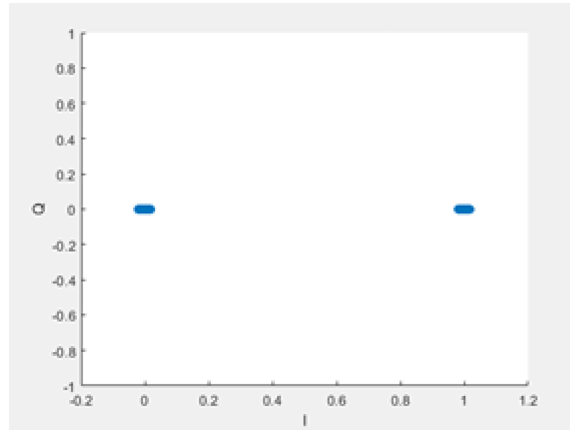

(b)

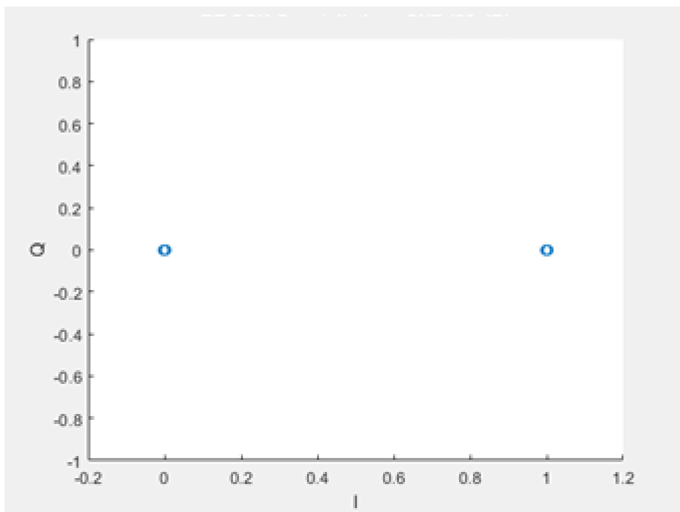

(c)

Figure 4.1: The OOK constellation diagrams for various SNR levels where the SNR is 4 dB in (a), 12 dB in (b), and 20 dB in (c) for the LP_{12} mode.

By increasing the SNR, the output of the match filter for different experiments are more concentrated around 0 and 1, which serves to verify the functionality of the proposed system. Figure 4.1 is to serve as a confirmation for the functionality of our system and its increasing accuracy in response to decreasing relative noise levels. The formulation of this sort can be extended for our ML detection algorithm to create an 2^N-dimensional constellation diagram where N is the number of modes. Additionally, we can scale down inside to see how the performance of the modes is affected by the worsening of sampling resolution.

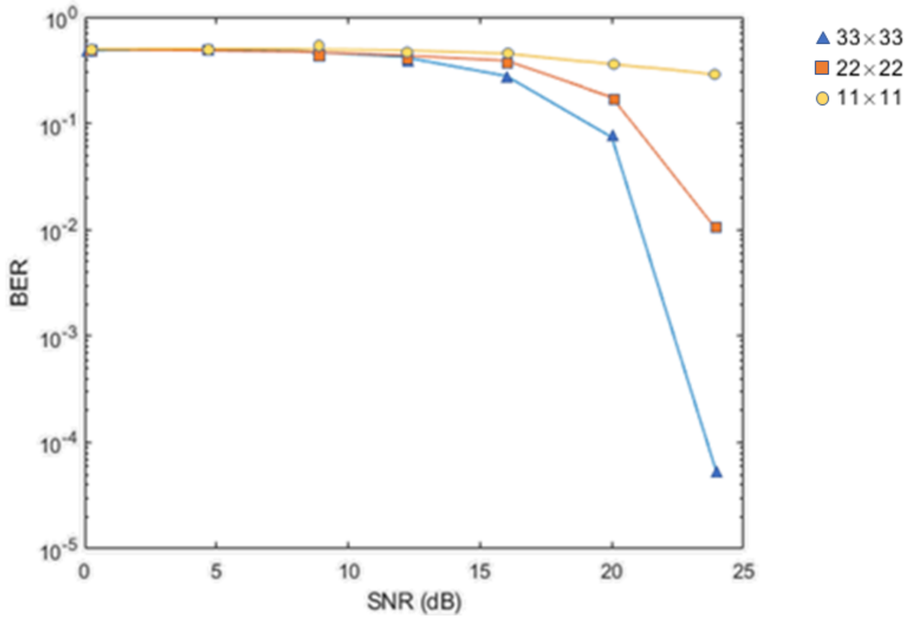

Figure 4.2: BER with decreasing spatial sampling frequency for an LP_{12} mode according to the parameters aforementioned parameters.

When the photodetector array grid sizes progressively decreases, it affects the performance of the system as shown in Figure 4.2. As we mentioned in Chapter 1, having a sensor low sampling rate can be a problem. Additionally, sampling too much the cladding can also be a problem due to extreme sensitivity to perturbation given the almost nonexistent optical energy in the cladding region. Here we only measured the ability to spatially correlate NRZ-OOK in optical field profiles; these pulses were simply square, not Gaussian. Our focus here is the successful transmission and correlation of optical spatial profiles. Each pulse would be represented by only one "page" in the time axis of Figure 3.6. An optical '1' would be the spatial profile in question and the optical '0' would simply be a noisy signal. In a sense, we would have a NRZ-OOK spatially correlating optical system. This section mainly talks about the results of this project as done in stages. We first start with spatial correlation with regard to perfectly square pulse where $T_s = T_b$. As most communications sample in time, it is important to first establish a basis for spatial correlation and reconstruction.

4.2 Application of Modal Analysis

The parameters mentioned at the introduction of this chapter yield the HE_{21}, TE_{01}, and TM_{01} modes, which are themselves degenerate, giving us the fundamental LP_{11} mode. They also yield the HE_{11} mode, which gives us the LP_{01} mode, and the HE_{12} mode is stimulated, giving us the LP_{02} mode. These three LP modes all have different group delays as given by the equation for the weakly-guided approximation for the group delay for $LP_{\nu m}$ modes:

$$\tau_{\nu m} = \frac{N_g}{c}\left(1 + \Delta\left(\frac{2m + \nu + 1}{n_{cl} k_0 a}\right)^2\right) \tag{4.1}$$

where N_g is the group index, n_{cl} is the index of the cladding, k_0 is the wavenumber, a is the radius of the core, c is the speed of light, Δ is the relative index difference, and ν and m are the azimuthal and radial orders, respectively [2,31].

When we evaluate our results, we evaluate the system performance when we integrate the temporal coefficient in time—which is the Gaussian pulse—into the system. In testing this system in our total evaluation of the signal, the drive was to feasibly reject Lau's assumption in [30] that the bit delays are integer multiples of bits. The way this was done was by using a matched filter to bypass the problem of modal path differentials. This will be explained in more detailed in a later section of this chapter. However, it important to note that the context of few-mode fibers and the weakly-guiding approximation allows for a small delay spread that preserves an effective temporal alignment for modes but is still integrable and manageable in the context our proposed architecture.

4.3 Modal Decomposition Method

In order to implement this system successfully we had to understand the principles of multiuser detection. Additionally, we divided the system into three methods. The first was in the context of an single core-fiber (SCF), the second was in the context of a multicore fiber (MCF), two were related to spatiotemporal OOK described in in Section 4.1 with emphasis on the mode profile and signal decomposition; the third was based on taking the signal as a whole. In this section we rely on a method of using an optical prism to use principles of geometric optics to split the signal into its modal components as demonstrated in Figure 1.9. What we do with our model is a typical MDM system combined with a typical temporally based communication system architecture. For one mode, we have a collection of users; consequently, it would take the following form:

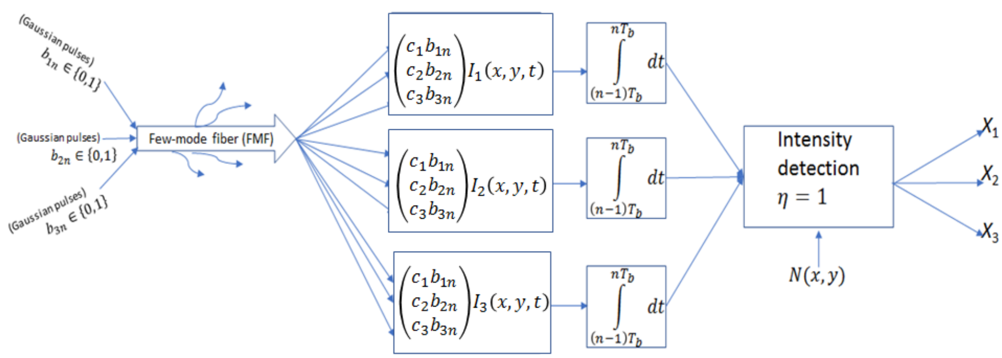

Figure 4.3: Model of a fiber optic multiuser system and the detection apparatus using a "integrate and dump" method in time.

Figure 4.3 represents multiple users over a single channel with different gains determined by their respective input offsets. Additionally, $I_k(x, y, t)$ represents the kth spatiotemporal modal correlator that would be used to correlate the pulses as they come through. Furthermore, we can generalize this to multiuser systems in MMFs to handle modal mixing, but such a task is beyond the scope of this thesis. For K bitstreams and N modes (channels), the users' nth bit functions as a single vector of bits. For classic multiuser detection the output bit matrix is expressed as

$$\vec{y}_{nm} = \boldsymbol{C_n}\vec{\mathrm{b}}_m + \vec{N}_{nm} \tag{4.3}$$

where $\boldsymbol{C_n}$ is the user matrix denoting the stimulation coefficients for the *n*th mode, $\vec{\mathrm{b}}$ is the bit vector per user for the *m*th bit, and $\vec{N}$ is the corresponding noise vector. We design $\boldsymbol{C_n}$ as our channel matrix, a diagonal matrix with deliberately distinct entries such that

$$\boldsymbol{C_n} = \begin{bmatrix} c_{n1} & 0 & \dots & 0 \\ 0 & c_{n2} & \dots & 0 \\ \vdots & \vdots & \ddots & \vdots \\ 0 & 0 & \dots & c_{nK} \end{bmatrix} \tag{4.4}$$

Here we would typically include a cross-correlation matrix $\boldsymbol{R_n}$ that measures the cross correlation of the pulse-shapes between users. However, such a matrix is not necessary since we assign the same Gaussian pulse-shape to each user so that pulse overlaps over the relevant bit periods have the same values. We achieve a quasi-orthogonality between the pulse-shapes such that $\boldsymbol{R_n} \underset{\sim}{\propto} \boldsymbol{I_n}$. In this case, we do not need multiuser detection as the bit streams do not mix. We successfully optimize for the users of this system in Table 3.1 and the results of that optimization are displayed in later figures.

4.4 System Architecture

Our first result is for measuring the proficiency of the spatial matched filters in how they correlate modal profiles. Then our second step was to integrate this into a temporal “integrate and dump” correlating receiver. Now our step is to map out the architecture of our multiuser detection system. For the SCF we have user coupling for each mode. In this paradigm the ideal energy of a particular user-symbol for user *n* matched to mode LP_{vm} is approximately defined by

$$E_{s,vm} \approx \frac{\tau_p}{2}\sqrt{\frac{\pi}{\ln 2}}\left|b_1 c_{1,vm} + b_2 c_{2,vm} + b_3 c_{3,vm}\right|^2 P_0 \tag{4.5}$$

The $c_{n,vm}$ values are the coupling coefficients for the n^{th} user given a particular radial offset, the value(s) b_k is the bit for the k^{th} user. These coupling values are computed by measuring the coupling of a Gaussian beam from a user's laser into the fiber. In the earlier experiments and trials with purely spatial matched filters, we used a purely SISO scheme. This method relied on a binary way of detecting bits—by a spatial correlation or a sufficient lack thereof (Figure 4.1). There are, however, two ways in which this multi-user system can be tested. One is through user reliability, i.e., the BER measured for a particular user. The other is the matched filter proficiency, which measures the symbol-error rate (SER) of a modally matched filter correlator. Our results measured both simultaneously. In order to bridge the two methods, we created an optical look-up table (LUT) for this model wherein the energy received was matched to a certain value of the user bit combinations. The decomposition of the signal into its constituent modes allows for an independent analysis of the "performance" of each mode by a sensor grid. Each sensor grid is to be placed at precisely calculated points outside the prism based on the index of refraction of the mode in the prism and its consequent trajectory therein.

4.5 System Performance Analysis

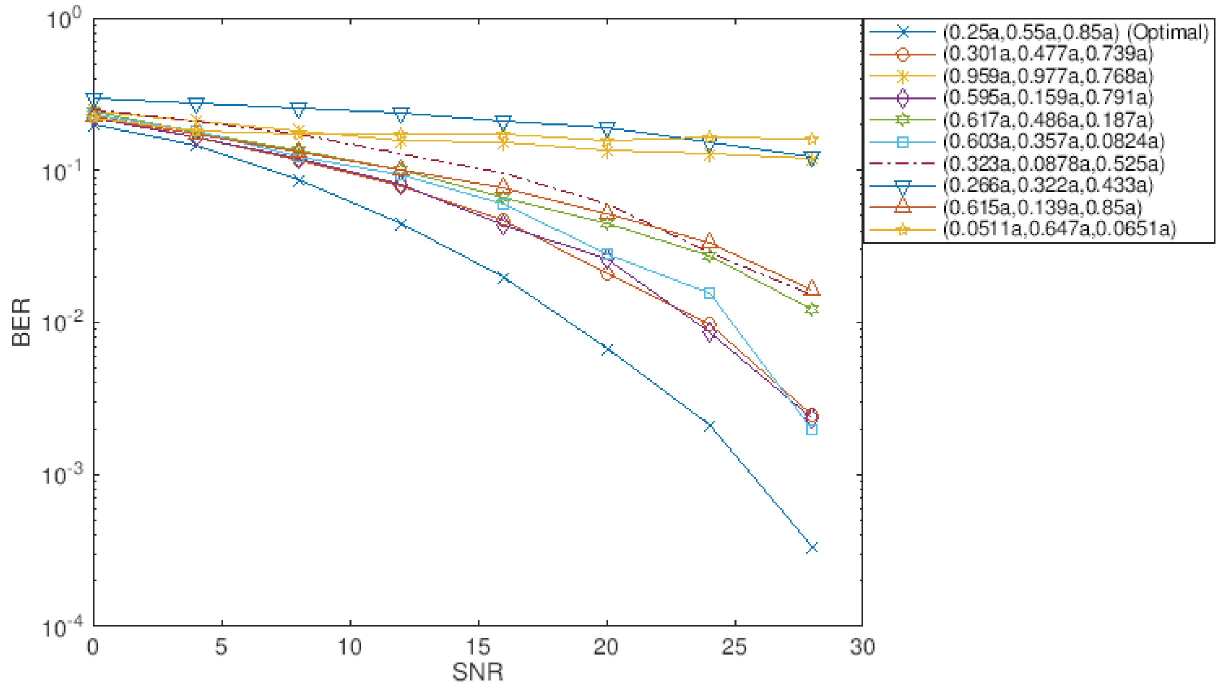

Figure 4.4: The performance of the system for different user settings showing the sensitivity of performance to user conditions.

The results in Figure 4.4 are explained by trials of different users and thus different laser input offset conditions with each trial. The figure shows an interesting dilemma in evaluating the matched filter performance which is the problem of the 'unlucky user(s)'. This corresponds to user settings where the optical LUT generated is more susceptible to corruption at different levels. While the overall trend for the BER would be downward for increasing SNR, the negative curvature of the BER-SNR measurement is a function of the initial conditions of the users. This is especially true if the system has a different set of users over different SNRs. In contrast, Figure 4.5 shows the results over the *same* set of arbitrarily positioned users.

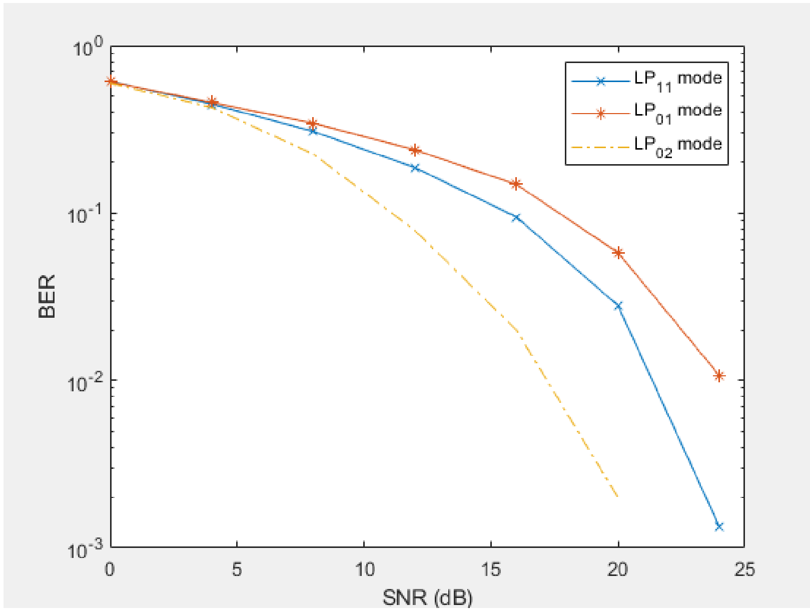

Figure 4.5: The modal results for the matched filter correlators over a single user set.

Figure 4.5 describes a set of users with radial offsets of $\rho_1 = 3.5$ µm, $\rho_2 = 4.8$ µm, and $\rho_3 = 2.7$ µm for users 1, 2, and 3, respectively. The performance differs with each mode but it is nevertheless superior to the Lau's result, reproduced in Figure 4.6 for the reader's convenience with the grid array.

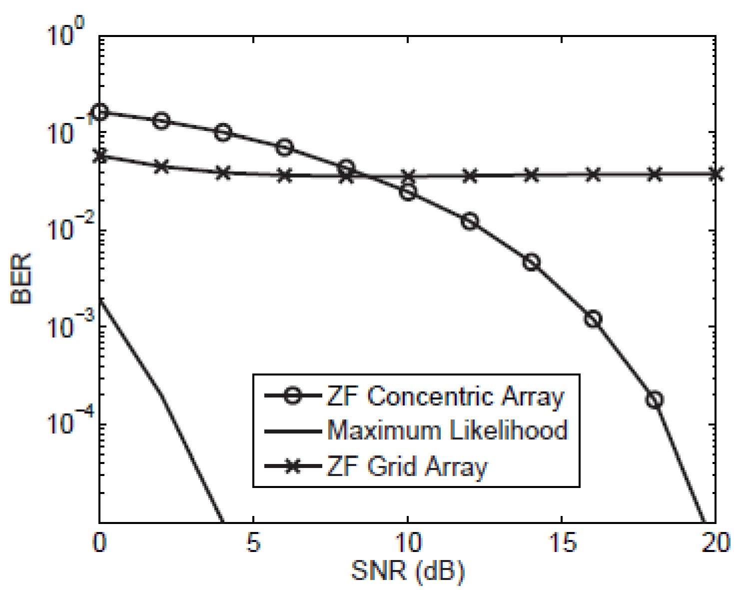

Figure 4.6: Lau's BER vs. SNR result for a series of detection apparatuses [30].

In Figure 4.6 there is a relevant comparison with the ZF grid array, where multiuser interference is nulled, denoted by the **x**'s. It expresses a *barely* downward trend with increasing SNR before hitting a limit. As was previously demonstrated, one of the problems that confronted us was the inconsistency in performance when testing for the reliability for each mode. As a result, we crafted a way to reduce the probability of symbol errors by maximizing the minimum energy differences in our optical LUT over all possible users as done in Section 3.5. This led to a user-friendly preset that we named our optimal user-preset enumerated in Table 3.1.

However, it should be noted that how one optimizes can also depend on *how* one chooses to multiplex. If one wants to compensate for the intermodal path delays to have the modes arrive at the simultaneously, then the corresponding LUT for multiuser detection will be different and the user-preset for performance optimization would also be different.

It would be necessary to find a way to get the modes on as much of a comparable level of stimulation as possible. Given the offset-dependent modal stimulation illustrated on the next page in Figure 4.7, such a way would have the modes stimulated by placing the users close to each other and towards to the edge of the fiber core near the cladding.

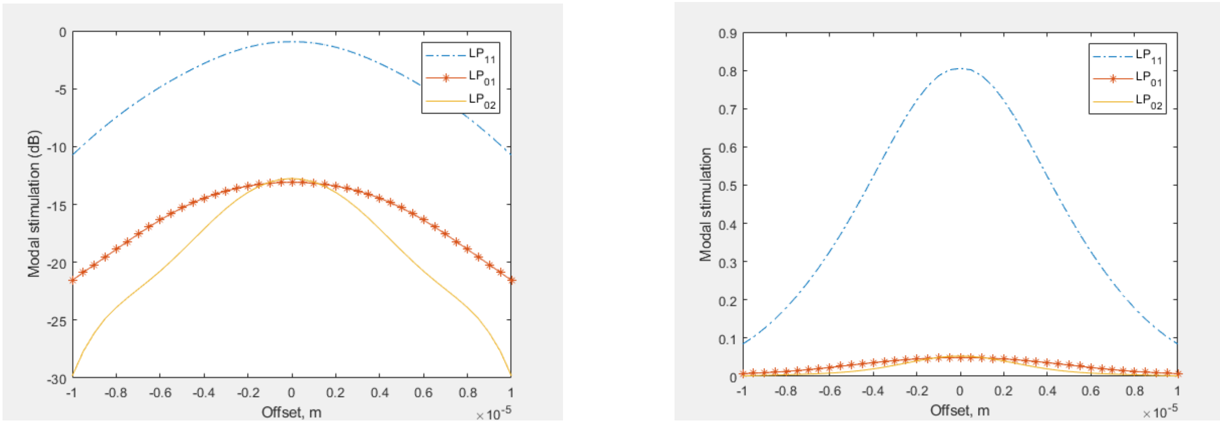

(a) (b)

Figure 4.7: The excitation coefficients $|c_{\nu m}|^2$ for the LP$_{\nu m}$ modes as a function of radial offsets in the *y*-direction for the LP$_{11}$, LP$_{01}$, and LP$_{02}$ modes in dB (a) and normalized units (b).

These "cladding presets" were based on a system where $\frac{d|c_{\nu m}|^2}{d\rho}$ is high and the values of $|c_{\nu m}(\rho)|^2$ is also fairly comparable. However, what most important here is that the values are sufficiently different for *each* mode. With his multiuser detection method the values of $|c_{\nu m}|^2$ do not have to be large enough, but rather *comparable* for user-symbol distinguishability.

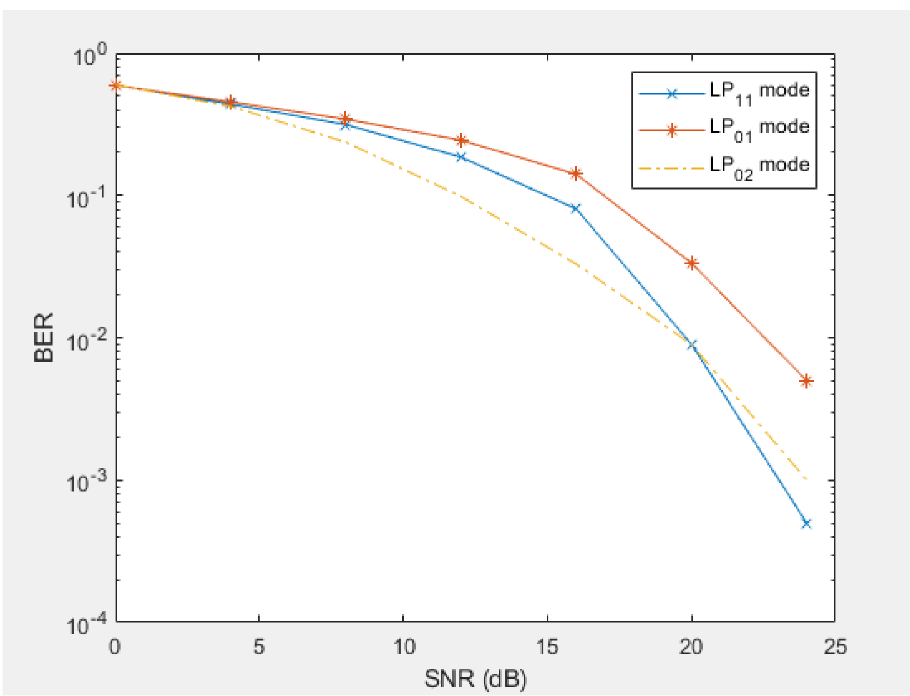

Figure 4.8: The results for the matched filter correlators for modes LP$_{11}$, LP$_{01}$, and LP$_{02}$ for an attempted optimization of user settings.

The cladding presets in Figure 4.8 are $\rho_1 = 9$ μm, $\rho_2 = 9.5$ μm, and $\rho_3 = 10$ μm for users 1, 2, and 3, respectively. With these offesets, there were better results, however, the excitation efficiencies for various modes can be manipulated to come up with an optimal coupling. The corresponding user excitation coefficients for each user is given in Table 4.1. Returning to the temporal domain we see that the temporal frequency response for this fiber optic channel is

$$|H_n(f)|^2 = \left|c_{11}(\rho_n)e^{-j2\pi f\tau_{g,11}L} + c_{01}(\rho_n)e^{-j2\pi f\tau_{g,01}L} + c_{02}(\rho_n)e^{-j2\pi f\tau_{g,02}L}\right|^2 \qquad (4.6)$$

as presented in Figure 4.9.

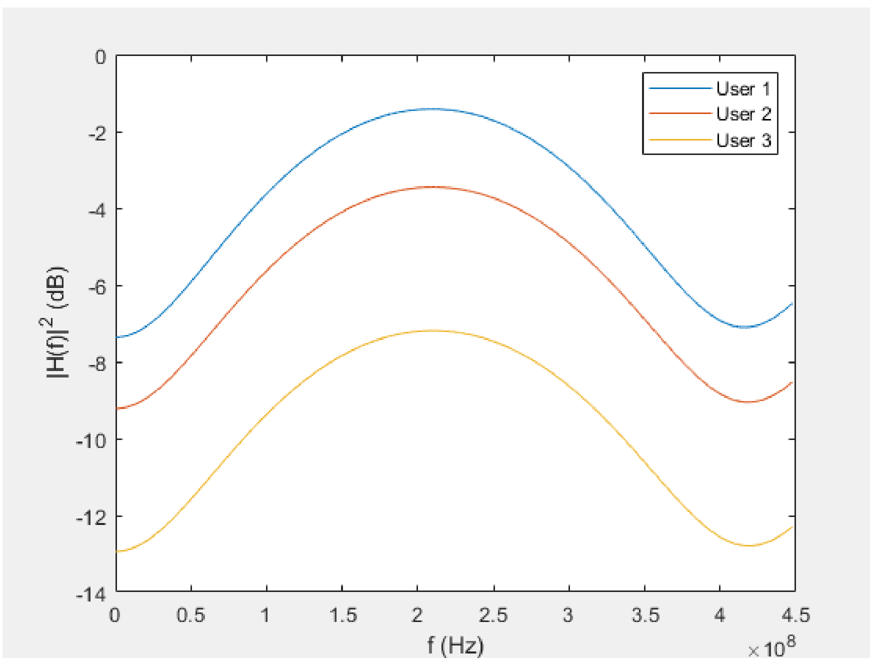

Figure 4.9: The channel frequency repsonses for each user according to the system offsets enumerated in Table 4.1.

Table 4.1: User-specific Modal Insertion Losses for Optimized System Parameters

User	***y*-offset-ρ (μm)**	**LP11 $\lvert c_{11}\rvert^2$**	**LP01 $\lvert c_{01}\rvert^2$**	**LP02 $\lvert c_{02}\rvert^2$**
User 1	± 2.5	0.6779	0.0436	0.0347
User 2	± 5.5	0.3712	0.0263	0.0102
User 3	± 8.5	0.1505	0.0111	0.0033

4.6 System Results—Single-core Fiber (User Interference)

In the previous system evaluation, we optimized for our single-core few-mode fiber scenario. In this section we test that optimization. In the employment of SCFs, we will have user-interference, which is mathematically signified the instance of cross-terms which basically function as a form of interference. Moreover, these terms generate two types of interference: intermodal interference and inter-user interference. Our analysis deepens in this iteration of performance-evaluation. While operating under the assumption of quasi-orthogonality between LP modes we additionally use a prism to separate modes at the end of the fiber. In this way, only inter-user interference at each mode is evaluated. We can express the *k*th bit and their corresponding modal excitation coefficients as matrices of the form

$$B_k = \begin{bmatrix} b_{k,1} & 0 & 0 \\ 0 & b_{k,2} & 0 \\ 0 & 0 & b_{k,3} \end{bmatrix} \leftrightarrow C_{vm} = \begin{bmatrix} c_{vm,1} & 0 & 0 \\ 0 & c_{vm,2} & 0 \\ 0 & 0 & c_{vm,3} \end{bmatrix}, \tag{4.7}$$

respectively. In this respect we can express field "weight" of the *k*th bit in time as $\mathrm{Tr}(B_k C_{vm})$, where $\mathrm{Tr}(\cdot)$ denotes a matrix's trace, i.e., the sum of the diagonals. In forcibly quelling modal interference, we instead use the user cross-terms at the square law detector. Ignoring noise, the total electric field transmitted is defined as

$$E_t(r,\phi,z,t) = \sum_{k=1}^{K} \mathrm{Tr}(B_k C_{11}) E_{11}\big(r,\phi,t-kT_b-\tau_{wg,11}L\big) e^{-j\beta_{11}z} \tag{4.8}$$

$$+ \mathrm{Tr}(B_k C_{01}) E_{01}\big(r,\phi,t-kT_b-\tau_{wg,01}L\big) e^{-j\beta_{01}z}$$

$$+ \mathrm{Tr}(B_k C_{02}) E_{02}\big(r,\phi,t-kT_b-\tau_{wg,02}L\big) e^{-j\beta_{02}z}$$

Then we solve for the intensity for our square-law detector for the modal matched filter for the modes. The intensity of the modes is taken into consideration for the cross-terms between users.

$$I(r,\phi,z,t) = \frac{n_c \varepsilon_0 c}{2} \sum_{k=1}^{K} \mathrm{Tr}(B_k C_{11})^2 \left| E_{11}\big(r,\phi,t-kT_b-\tau_{wg,11}L\big) \right|^2 \tag{4.9}$$

$$+ \mathrm{Tr}(B_k C_{01})^2 \left| E_{01}\big(r,\phi,t-kT_b-\tau_{wg,01}L\big) \right|^2$$

$$+ \mathrm{Tr}(B_k C_{02})^2 \left| E_{02}\big(r,\phi,t-kT_b-\tau_{wg,02}L\big) \right|^2$$

In setting the energy weights we get the following intensity for each of the respective matched filters, the modal delays being considered. Our new threshold is

$$I_{11}(r,\phi,z,t) = \frac{n_c \varepsilon_0 c}{2} |E_{11}(r,\phi,z,t)|^2 \left\{ \sum_{k=1}^{K} \left(\left|b_{k,1} c_{11,1}\right|^2 + \left|b_{k,2} c_{11,2}\right|^2 + \left|b_{k,3} c_{11,3}\right|^2 \right) \right. \tag{4.10}$$

$$+ 2 \sum_{i \neq j}^{K} b_{i,1} b_{j,2} \left| c_{11,1} c_{11,2} \right| \cos\big(\theta_{11,1} - \theta_{11,2}\big)$$

$$+ b_{i,1} b_{j,3} \left| c_{11,1} c_{11,3} \right| \cos\big(\theta_{11,1} - \theta_{11,3}\big)$$

$$\left. + b_{i,2} b_{j,3} \left| c_{11,2} c_{11,3} \right| \cos\big(\theta_{11,2} - \theta_{11,3}\big) \right\}$$

$$I_{01}(r,\phi,z,t) = \frac{n_c \varepsilon_0 c}{2} |E_{01}(r,\phi,z,t)|^2 \left\{ \sum_{k=1}^{K} \left(\left|b_{k,1}c_{01,1}\right|^2 + \left|b_{k,2}c_{01,2}\right|^2 \right. \right.$$

$$\left. + \left|b_{k,3}c_{01,3}\right|^2 \right)$$

$$+ 2\sum_{i\neq j}^{K} b_{i,1}b_{j,2}\left|c_{01,1}c_{01,2}\right| \cos\left(\theta_{01,1} - \theta_{01,2}\right)$$

$$+ b_{i,1}b_{j,3}\left|c_{01,1}c_{01,3}\right| \cos\left(\theta_{01,1} - \theta_{01,3}\right)$$

$$\left. + b_{i,2}b_{j,3}\left|c_{01,2}c_{01,3}\right| \cos\left(\theta_{01,2} - \theta_{01,3}\right) \right\} \tag{4.11}$$

$$I_{02}(r,\phi,z,t) = \frac{n_c \varepsilon_0 c}{2} |E_{02}(r,\phi,z,t)|^2 \left\{ \sum_{k=1}^{K} \left(\left|b_{k,1}c_{02,1}\right|^2 + \left|b_{k,2}c_{02,2}\right|^2 \right. \right.$$

$$\left. + \left|b_{k,3}c_{02,3}\right|^2 \right)$$

$$+ 2\sum_{i\neq j}^{K} b_{i,1}b_{j,2}\left|c_{01,1}c_{01,2}\right| \cos\left(\theta_{01,1} - \theta_{01,2}\right)$$

$$+ b_{i,1}b_{j,3}\left|c_{01,1}c_{01,3}\right| \cos\left(\theta_{01,1} - \theta_{01,3}\right)$$

$$\left. + b_{i,2}b_{j,3}\left|c_{01,2}c_{01,3}\right| \cos\left(\theta_{01,2} - \theta_{01,3}\right) \right\} \tag{4.12}$$

The $\cos(\cdot)$ components come from the fact that the excitation amplitudes are complex numbers due to the complex spatial profile of the Laguerre-Gaussian beam that stimulates them. However, for our purposes we have each laser touching the entrance of the fiber so that the radius of curvature $R(z)$ goes to infinity and there is no imaginary component to the electric field profile as described in Equation 1.4. This does not fix everything as the field signal is still a complex bandpass signal so we additionally assume that the users function as branches of the same laser so that the relative phase coming into the fiber is also zero. Consequently, the $\cos(\cdot)$ components of the cross-terms all possess a value of unity. Additionally, we approximate the index of refraction to be n_c everywhere due to the weakly-guiding approximation. For each mode detector the energy received is described thusly:

$$E_b \propto \frac{\tau_p}{2}\sqrt{\frac{\pi}{\ln 2}}\left|b_{n1}c_{1,\nu m} + b_{n2}c_{2,\nu m} + b_{n3}c_{13\nu m}\right|^2 P_0 \tag{4.13}$$

Our first testing of this system the isngle-user excitation of one mode where the pulse was purely rectangular. The prismatically-mediated modal orthogonalization of the signal makes user-interference intrinsic to the spatiotemporal correlator for each mode. It subsequently brings the allocation of beam-offsets for the users into focus to distinguish between various levels for certain user symbols. Our experiment for the SCF builds on the aforementioned tests and results in dealing with the complexities of user interference, its effect on performance, and optimization within that paradigm.

In Figure 4.8 we ran the system according to a guess of which settings would yield the best results based on where the modal IL changed the most rapidly with beam-offest. However, when we optimized for the cross-terms in Table 3.1 in Section 3.5, we got the optimal offset parameters of $\rho_1 = \pm 2.5$ µm, $\rho_2 = \pm 5.5$ µm, and $\rho_3 = \pm 8.5$ µm. Figure 4.10 figures below show the results of that optimization.

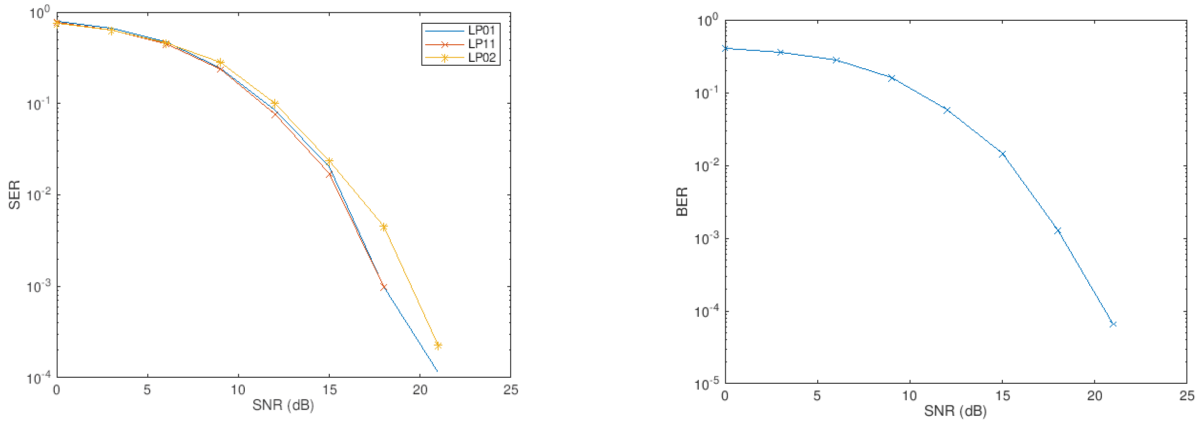

(a) (b)

Figure 4.10: The optimized modal (a) (SER) and system (b) performances (BER) of the matched filters in the context of an SCF.

We additionally were able to generate a user-specific assessment of the system. Here we measure the BER by demultiplexing the user-symbols. Here we get a picture of the system performance as perceived by the individual modes.

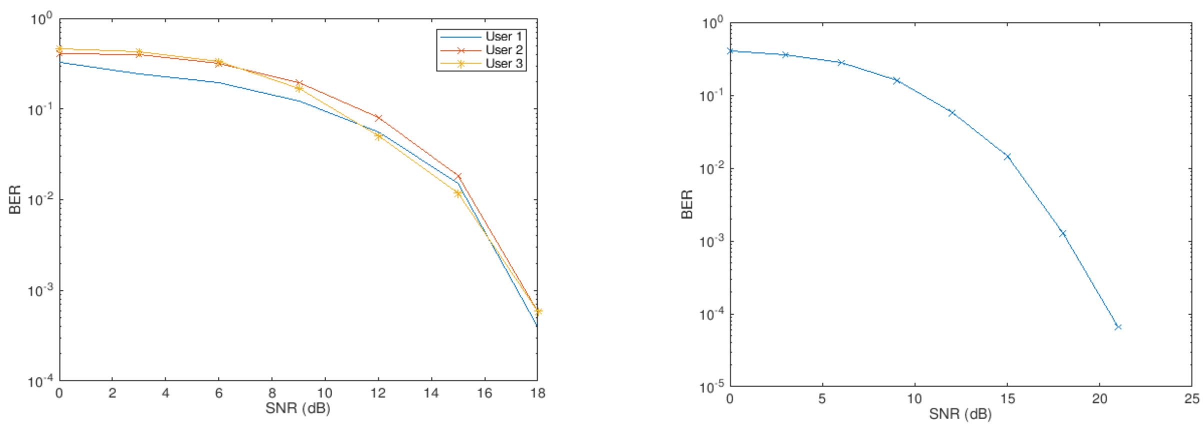

(a) (b)

Figure 4.11: The optimized user (a) and system (b) BER performances of the matched filters in the context of an SCF.

In considering the cross terms that arise between users for a particular matched filter, we saw that there was still good performance. However, this is clearly not as good as the MCF performance where the BER reached 10^{-4} when the SNR was at 14.75 dB. In the SCF the BER reaches the same point when the SNR is at 20.58 dB. The non-degeneracy of user symbols was also implicated not only because of the aforementioned offsets, but also because of what 1 or 0 means *for each* user-symbol, which includes inter-user interference. In order to get a more holistic picture of the system, more work needs to be done with intermodal coupling, where differences in arrival time must be considered due to modal dispersion. However, we can synchronize these modes using an a priori accounting for the delay between modes.

Unlike Lau in [40], we did not use correlators for the modal cross terms, which would have surely increased complexity more. We only took into account the performance of the directly stimulated modes and did this through externally mediated decomposition.

In this implementation of the system, we demonstrate the working principles of an integrative architecture for doing optical communication by multiplexing in the spatial and temporal regimes, spatially correlating the optical mode profiles and temporally integrating Gaussian pulses. Both systems create a simultaneous bit-checking algorithm that measures spatiotemporal correlations. The performance is a success because it makes user-interference caused by our directly detecting square-law photodetector grids a part of an optical look up table. It is worth noting also that the users and the modal matched filter correlators have roughly the same performance, showing robustness on the individual modal and user level and on a broader systemic level.

4.7 System Results—Multicore Fiber (User Orthogonality)

We achieve user orthogonality here in a multicore fiber. We have three cores as this model includes three users. Here we make use of a multicore fiber (MCF) where each core is an single-mode fiber (SMF) core. This work exists in the context of crafting novel techniques for the facilitation of SDM. This combination of users and modes leads to a total of three orthogonal spatial channels. In this way there would be no need for multiuser detection. The values for our mode specific LUT here would be described by the coupling of the Gaussian beam to the fundamental mode. In this scheme one need not optimize for the user-preset. The fundamental mode can be stimulated in all three modes with the same offset.

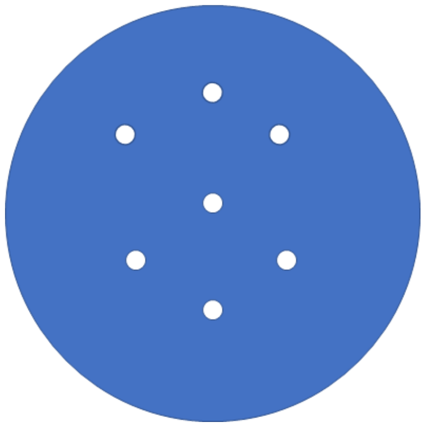

Figure 4.12: Model of multicore fiber, one and mode core per user.

Figure 4.12 shows a model of a multicore fiber (MCF) with optimal core spacing for low crosstalk. When we work in the 'absence' of user coupling we assume that we have the users in separate channels—i.e. no crosstalk between users.

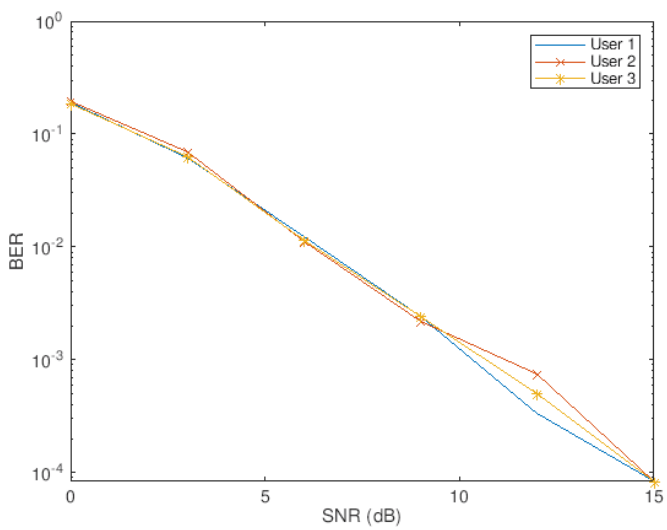

Figure 4.13: The user performances (BER) of the system in the context of an MCF.

The result in Figure 4.13 is what it would mean for the system to work in a multicore fiber with one user per fiber core at zero offset. The figure assesses the performances of all among the users of the MCF system. The comprehensive system performance is determined through averaging the performances of the users. The performance of the system makes sense given the independence of the users and the fact that they each excite the fundamental mode of the fiber. All conditions remain the same except the index refraction of the cladding n_{cl}, which has been changed from 1.497 to 1.498, thereby decreasing the numerical aperture *NA* from .0948 to .0774. The MCF system employs the lowest order of detection, binary detection. However, things change when we scale up to put multiple users through the same fiber channel and hence the comparatively worse performance. Comparing the two methods—as we do in Figure 4.14—shows a clear advantage in using an MCF.

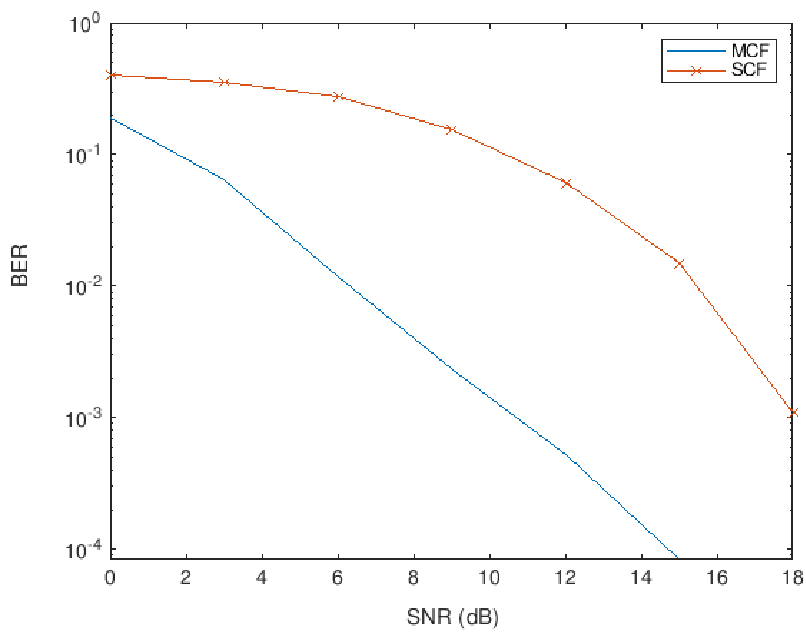

Figure 4.14: Comparison of optimized multiuser system for MCF and SCF.

As shown in Figure 4.14, the MCF reaches a BER of 10^{-3} at around 10.75 dB whereas the SCF reaches the same point at around 18 dB.

4.8 System Results—Intermodal Convolution

The first test used a receiver prism to act as a decomposition system that decomposed the individual path (mode) components of the system. The second test was an implementation of the system in way that the users are independent. Our final test is to take the entire system as a whole. This means including the cross-terms that arise from the differences in β-values for the LP modes using a PD array without the prism. When we combined the whole system with regards to the square-law detector we get

$$I_m \approx \frac{n_c \varepsilon_0 c}{2} \left| \sum_n \mathrm{Tr}(C_n B_m) E_n(r, \phi, t - \tau_n L) e^{-j\beta_n L} \right|^2 \tag{4.14}$$

where C_n is the matrix describing the user-specific excitation amplitudes of the *n*th mode and *B* is the diagonal matrix that denotes the *m*th set of bits among the users. This gives us a total symbol energy of

$$E_s \approx \frac{n_c \varepsilon_0 c \tau_p}{4} \sqrt{\frac{\pi}{\ln 2}} \iint \left| \sum_n \mathrm{Tr}(C_n B) E_n(r, \phi, t - \tau_n L) e^{-j\beta_n L} \right|^2 r dr d\phi \tag{4.15}$$

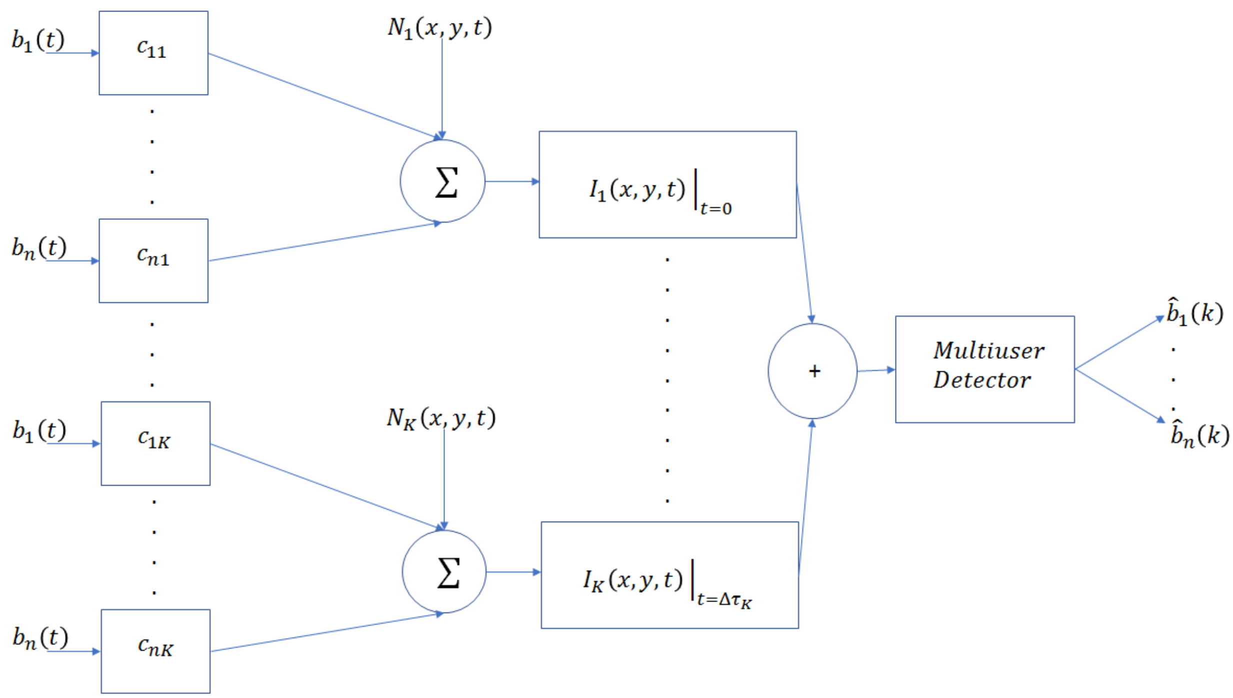

Figure 4.15: A diagram of an n-user multiuser system with K eigenchannels, or modes, where $\Delta\tau_K$ is the *relative* delay for a particular mode.

Figure 4.15 shows the implementation of the system where all the relative time delay differences are summed together as one single signal. As we previously said, we can treat the fiber channel system as a multipath channel in that it contains its own echoes. Furthermore, we can use channel estimation to estimate the values of our time delays τ_n. In this way we can dynamically process our data stream with its modal echoes. This is done by understanding at which points the echoes overlap with each other. In a fiber with N path delays one can identify $2N-1$ zones where the detection algorithm will have to be adjusted. Given N path delays, there will be $N-1$ adjustments for the paths as they begin being received one-by-one, one adjustment for when they are all simultaneous, and $N-1$ for when their individual streams end. This yields $2N-1$ adjustments, or 5 since we are dealing with multipath channel of $N=3$.

In incorporating the temporal delay of the pulses over our fiber length of $L = 25$ km, we found that the LP_{02} mode has the shortest duration through the fiber of $\tau_{01} = 124.64862$ μs, the LP_{01} mode has a duration through the fiber of $\tau_{02} = 124.64775$ μs, the LP_{11} mode has a duration through the fiber of $\tau_{11} = 124.940650$ μs. The problem becomes seemingly difficult when we reject the idea that the delays are integer numbers of bits. However, this is not necessarily so. The LUT generated is a product of the noiseless signal passing through the fiber. Whatever form this signal takes will generate a certain amount of unique values to which we can compare our signal when sampling over the bit interval of length $2\tau_p$.

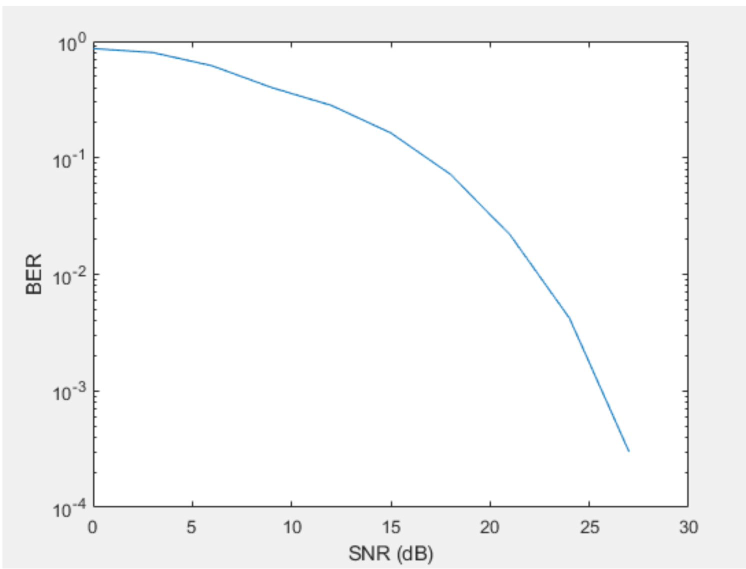

Figure 4.16: The BER vs. SNR for the non-decomposed fiber channel bit-stream.

Figure 4.16 shows that compared to our previous to systems, this implementation of the system where no decomposition takes place has the worst performance as it reaches a BER of 10^{-3} at an SNR of approximately 26.4 dB. We have tested the system in both multicore and single-core contexts. However, both of methods of testing relied on some sort of signal decomposition. In order to do this at high performance, more channel information must be gleaned to understand how much of a particular mode is present and when it should be expected in the signal.

There are a few ways to treat the multiuser mode-specific optical multichannel transmitter described in Figure 4.15. We could sum the whole system together as one and as the Gaussian beams that are input excite multipath responses in the fiber. We can thus treat the modal channels as roughly orthogonal in this respect. We do this in the context of a single core fiber so there will be user coupling. Our spatial temporal matched filter takes the form

$$E^{*}(r,\theta,t) = E_{vm}(r,\theta)e^{-\ln 4\left(\frac{t}{\tau_p}\right)^2}\sum_{n=1}^{N} c_n b_n\,, \qquad -\tau_p < t < \tau_p \tag{4.16}$$

$$I^{*}(r,\theta,t) = I_{vm}(r,\theta)e^{-2\ln 4\left(\frac{t}{\tau_p}\right)^2}\left|\sum_{n=1}^{N} c_n b_n\right|^2, \qquad -\tau_p < t < \tau_p \tag{4.17}$$

where *N* is the number of users and c_n and b_n are the stimulation coefficients and the relevant bit-codes, respectively. The summations effectively function as modulation codes for the spatiotemporal signal templates.

In this new test, this is analogous to correlating a noisy video with the original. This matched filter would take the form of the three-dimensional matrix arrangement shown in the Figure 3.8 of the previous chapter. The same “pages” that denote the *t*-axis in Figure 3.8 would be scaled according to the requirements outlined in Chapter 2 regarding how much sampling per pulse is necessary according to an approximation of the Nyquist theorem.

4.9 Chapter Summary

In this chapter we have presented the results of our method of spatiotemporal correlation establishing benchmarks along the way that bolster the plausibility of combining space and time for communication. A method of turning a problem more associated with fiber optic imaging into one that is associated with communications is proposed. We demonstrate the working principles of an integrative architecture for doing optical communication by multiplexing in the spatial and temporal regimes, spatially correlating the optical mode profiles and temporally integrating Gaussian pulses. Both systems create a simultaneous bit-checking algorithm that measures spatiotemporal correlations. The photodetector grids take advantage of the detecting the intensity at properly sampled intervals. Additionally, we can reconfigure the information encoded onto the modes with this approach and this can occur with or without modal decomposition.

We assembled this architecture in three configuration stages. The first was in the presence of user coupling and prismatically induced modal orthogonality. The second was in the context of an MCF to deal with the physical constrains that would likely arise from a single-core fiber with multiple lasers competing for space. The orthogonality in this approach was beneficial for the performance of our system with a 3.25 dB SNR advantage when performing at a BER of 10^{-3}. We saw that our performances for the modes were selective based on the optimizing method described in Section 3.8 and that this optimization method worked as demonstrated in Figure 4.4. However, in both instances we were able to demultiplex the user-symbols to get the performances even though the splitting occurred at the level of the individual modes. The third method had the worst performance as it was more difficult to split the signal into its proper components given modal and user coupling. This is consistent with what we expected. Such a method is inefficient as well because it would require one matched filter for each of the modes stimulated *per user*. The second method shows more promise as the users are together in multiple cores with little to no cross talk.

The matched filter correlator is purely spatial. It is an addendum to more temporally based communication systems used today. Both this stage and the former make use of the "integrate and dump" method. This method wastes a lot of energy as it requires the filter correlator to be recreated for every bit. The third stage was a successful synthesis in the spatial and temporal domains in creating the matched filter without decomposing the signal even though more work needs to be done with that method. This approach used an appropriate matched filter correlator in space and time. The difference in the last method was a dynamic change in how detection occurred at different parts of the bitstream. This dynamically changing detection algorithm was a robust result of the channel estimation for our model. The correlation was done with a bit-stream modulating a particular mode in time; this bit-stream also *matched* the original bit-stream of the users in length. The correlation is still pulse-by-pulse but it is an entire pulse train that does the correlation. This method allows the spatial and temporal domains to feed off each other in determining user symbols. The incorporation of the delay time in this method allows for an analog delay for the expected time of propagation. In this way, the delay does not necessarily have to be an integer number of bit lengths.

With a robust performance validated in this system overall, we demonstrate a way forward for fiber optic communication systems by exploiting the spatial aspect of fiber optic signals, building upon existing communication architectures, providing a basic foundation for an "intelligent" optical communication system, and thus bridging the gap between imaging and communication for a more efficient system.

References

1. *"NEC and Corning achieve petabit optical transmission"*. Optics.org. 2013-01-22. Retrieved 2018-01-18.

2. S. Davis. *Precoder for Multimode Optical Fiber*. *Charlottesville*, Master's Thesis. University of Virginia. https://doi.org/10.18130/V39T0C

3. G. Stepniak, L. Maksymiuk and J. Siuzdak, "Increasing multimode fiber transmission capacity by mode selective spatial light phase modulation," *36th European Conference and Exhibition on Optical Communication*, Torino, 2010, pp. 1-3. doi: 10.1109/ECOC.2010.5621465

4. T. Morioka, "New generation optical infrastructure technologies," Proc. OECC, FT4 (2009).

5. J. T. Boyd and C. L. Chen, "Integrated optical silicon photodiode array," Appl. Opt. **15**, 1389-1393 (1976)

6. M. H. White, D. R. Lampe, F. C. Blaha, and I. A. Mack, "Characterization of surface channel CCD image arrays at low light levels", IEEE J. Solid-State Circuits **SC-9**, 1 (1974).

7. A. K. Majumdar, "Impulse response of a picosecond photodetector from power spectrum measurements", *Appl Opt.*, vol. 25, pp. 2041-2043, 1986.

8. Karel Hinnen, Michel Verhaegen, and Niek Doelman, "Exploiting the spatiotemporal correlation in adaptive optics using data-driven $\mathcal{H}_2$-optimal control," J. Opt. Soc. Am. A **24**, 1714-1725 (2007)

9. P. A. Andrekson and M. Westlund, "Nonlinear optical fiber based high resolution all-optical waveform sampling", Laser Photon. Rev. 1 (3), 231 (2007).

10. D. H. Auston and P. R. Smith, "Picosecond optical electronic sampling characterization of high speed photodetectors," Appl. Phys. Lett., vol. 4 1, 1982.

11. G. Berrettini, A. Bogoni, F. Fresi, G. Meloni, and L. Potì, "Evolution of optical sampling," in Advances in Lasers and Electro Optics, N. Costa and A. Cartaxo, eds. (INTECH, 2010), pp. 289–314.

12. Doms, M. (2003) "Communications equipment: what has happened to prices?", Working Paper No. 2003–15, Federal Reserve Bank of San Francisco.

13. K. Ohashi *et al*., "Silicon photodiodes," *3rd IEEE International Conference on Group IV Photonics, 2006.*, Ottawa, Ont., 2006, pp. 176-178. doi: 10.1109/GROUP4.2006.1708204

14. Pollock, C. R. “Step-Index Circular Waveguides.” Fundamentals of Optoelectronics, CBLS, 2003.

15. O’Brien, W. (2014). *Optoelectronics Lecture Notes* [PowerPoint slides]. Retrieved from https://www.slideshare.net/chinkitkit/chapter-2b-36657191

16. Pampaloni, F. and Enderlein, J. (2004). "Gaussian, Hermite-Gaussian, and Laguerre-Gaussian beams: A primer". arXiv:physics/0410021

17. Leon-Saval, S. G., Fontaine, N. K. & Amezcua-Correa, R. Photonic lantern as mode multiplexer for multimode optical communications. *Opt. Fibre Technol.* **35**, 46–55 (2017).

18. G. Ruffato, M. Massari, and F. Romanato, "Generation of high-order Laguerre–Gaussian modes by means of spiral phase plates," Opt. Lett. **39**, 5094-5097 (2014)

19. Nicolas K. Fontaine, Roland Ryf, Joss Bland-Hawthorn, and Sergio G. Leon-Saval, "Geometric requirements for photonic lanterns in space division multiplexing," Opt. Express **20**, 27123-27132 (2012)

20. T. A. Birks, I. Gris-Sánchez, S. Yerolatsitis, S. G. Leon-Saval, and R. R. Thomson, "The photonic lantern," Adv. Opt. Photon. **7**, 107-167 (2015)

21. Naidoo, D., Ait-Ameur, K., Brunel, M. & Forbes, A. *Intra-cavity generation of superpositions of Laguerre-Gaussian beams*. *Appl. Phys. B* **106**, 683–690 (2012).

22. J. W. Goodman, *Introduction to Fourier Optics* (McGraw-Hill Publishing Company, 1968).

23. W. V. Sorin, B. Y. Kim, and H. J. Shaw, "Phase-velocity measurements using prism output coupling for single- and few-mode optical fibers," Opt. Lett. **11**, 106-108 (1986)

24. I. Giles, A. Obeysekara, R. Chen, D. Giles, F. Poletti and D. Richardson, "Fiber LPG Mode Converters and Mode Selection Technique for Multimode SDM," in *IEEE Photonics Technology Letters*, vol. 24, no. 21, pp. 1922-1925, Nov.1, 2012.

25. Ronald L. Phillips and Larry C. Andrews, "Spot size and divergence for Laguerre Gaussian beams of any order," Appl. Opt. **22**, 643-644 (1983)

26. L. G. Cohen, C. Lin and W. G. French, "Tailoring zero chromatic dispersion into the 1.5-1.6 μm low-loss spectral region of single-mode fibres," in *Electronics Letters*, vol. 15, no. 12, pp. 334-335, 7 June 1979. doi: 10.1049/el:19790237

27. Abramowitz, Mortimer and Davidson, Michael W., (2000) Interline Transfer CCD Architecture. Concepts in Digital Imaging Technology.

28. T. Ishi, J. Fujikata, K. Makita, T. Baba, and K. Ohashi, "Si Nano-Photodiode with a Surface Plasmon Antenna," Jap. J. Appl. Phys., vol. 44, pp. L364-L366, 2005

29. Shanmugan, K. Sam. *Digital and Analog Communication Systems*. Wiley, 1979.

30. A. P. T. Lau, L. Xu, and T. Wang, “Performance of receivers and detection algorithms for modal multiplexing in multimode fiber systems,” IEEE Photon. Technol. Lett. 19 (14), 1087–1089 (2007).

31. A. Juarez, C. Bunge, S. Warm, and K. Petermann. “Perspectives of principal mode transmission in mode-division-multiplex operation.” *Optics Express*, vol. 20, no. 13, June 2012.

32. Fatih Yaman, Neng Bai, Benyuan Zhu, Ting Wang, and Guifang Li, "Long distance transmission in few-mode fibers," Opt. Express **18**, 13250-13257 (2010)

33. Papoulis, Athanasios (1981). *Systems and Transforms with Applications to Optics*. Florida USA: Krieger Publishing Company. pp. 140–175.

34. S. H. Murshid, J. Iqbal, "Array of concentric CMOS photodiodes for detection and de-multiplexing of spatially modulated optical channels", *J. Opt. Laser Technol.*, vol. 41, no. 6, pp. 764-769, Feb. 2009.

35. Masaaki Imai and Elmer H. Hara, "Excitation of the Fundamental and Low-Order Modes of Optical Fiber Waveguides with Gaussian Beams. 2: Offset Beams," Appl. Opt. **14**, 169-173 (1975).